

Modeling the impact of wind and waves on suspended particulate matter fluxes in the East Frisian Wadden Sea (southern North Sea)

Karsten A. Lettmann · Jörg-Olaf Wolff ·
Thomas H. Badewien

Received: 20 October 2008 / Accepted: 8 March 2009
© Springer-Verlag 2009

Abstract Suspended particulate matter (SPM) fluxes and dynamics are investigated in the East Frisian Wadden Sea using a coupled modeling system based on a hydrodynamical model [the General Estuarine Transport Model (GETM)], a third-generation wave model [Simulating Waves Nearshore (SWAN)], and a SPM module attached to GETM. Sedimentological observations document that, over longer time periods, finer sediment fractions disappear from the Wadden Sea Region. In order to understand this phenomenon, a series of numerical scenarios were formulated to discriminate possible influences such as tidal currents, wind-enhanced currents, and wind-generated surface waves. Starting with a simple tidal forcing, the considered scenarios are designed to increase the realism step by step to include moderate and strong winds and waves and, finally, to encompass the full effects of one of the strongest storm surges affecting the region in the last hundred years (Storm *Britta* in November 2006). The results presented here indicate that moderate weather conditions with wind speeds up to 7.5 m/s and small waves lead to a net import of SPM into the East Frisian Wadden Sea. Waves play only a negligible role during these

conditions. However, for stronger wind conditions with speeds above 13 m/s, wind-generated surface waves have a significant impact on SPM dynamics. Under storm conditions, the numerical results demonstrate that sediments are eroded in front of the barrier islands by enhanced wave action and are transported into the back-barrier basins by the currents. Furthermore, sediment erosion due to waves is significantly enhanced on the tidal flats. Finally, fine sediments are flushed out of the tidal basins due to the combined effect of strong erosion by wind-generated waves and a longer residence time in the water column because of their smaller settling velocities compared to coarser sediments.

Keywords Suspended particulate matter fluxes · Wadden Sea · Tidal flat · Surface gravity waves · Storm surges · Numerical modeling

1 Introduction

Long-term sedimentological observations have demonstrated that the sediment size distribution in the East Frisian Wadden Sea (see Fig. 1) has shifted towards coarser sediment fractions (Flemming and Nyandwi 1994). These observations are in conflict with the common assumption that fine-grained sediments accumulate in tidal flat systems due to effects like the settling/scour lag effect (van Straaten and Kuenen 1957) or density-driven effects (Burchard et al. 2008).

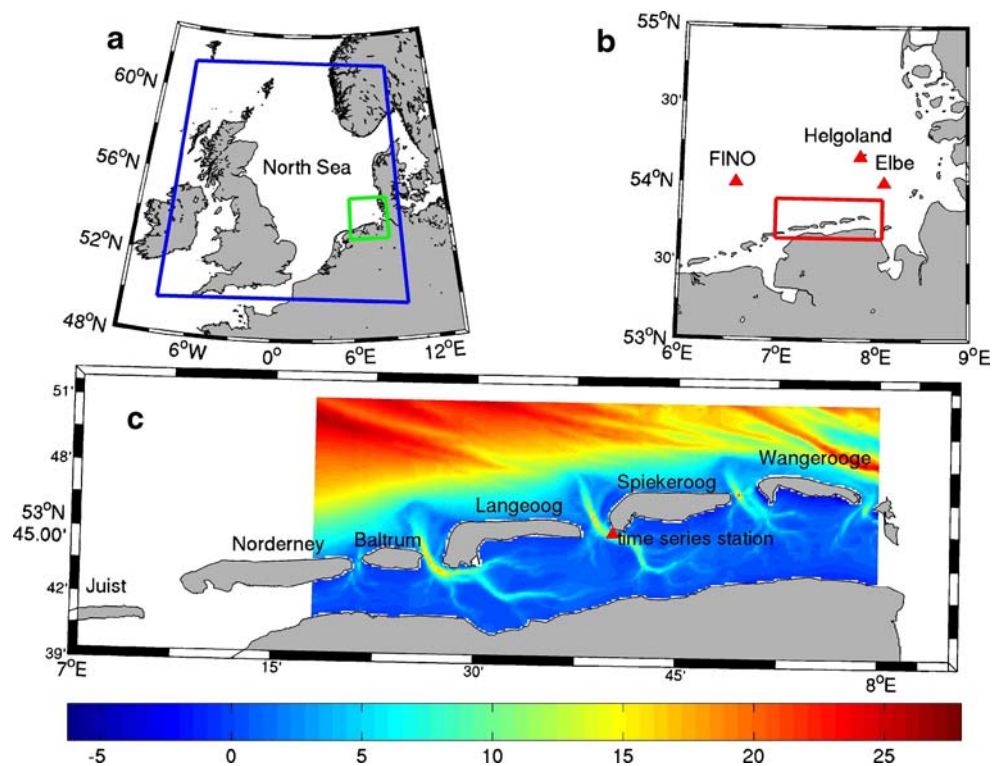
The observed deficit of fine-grained sediments in the East Frisian Wadden Sea must therefore be based on other mechanisms or a combination of mechanisms that overcome the accumulation tendency. Possible candidates influencing the suspended particulate matter

Responsible Editor: Ulrike Feudel

K. A. Lettmann (✉) · J.-O. Wolff
Institute for Chemistry and Biology of the Sea (ICBM),
Department of Physical Oceanography (Theory),
Carl von Ossietzky University Oldenburg,
Carl-von-Ossietzky-Str. 9-11, 26111 Oldenburg, Germany
e-mail: lettmann@icbm.de

T. H. Badewien
Institute of Physics, Department of Marine Physics,
Carl von Ossietzky University Oldenburg,
Carl-von-Ossietzky-Str. 9-11, 26111 Oldenburg, Germany

Fig. 1 Location of the study site and the model area. The model topography (positive downward, units in meters) of the Wadden Sea Model is depicted in **c**. The *red triangle* in that panel marks the position of the time-series station where wave parameters, sediment concentrations, and current velocities in the Wadden Sea area were measured. The *blue box* (**a**) denotes the extension of the model domain used for wave modeling in the North Sea area, whereas the *green box* outlines the extension of the model domain used for wave modeling in the German Bight. The *red triangles* in **b** denote the positions of the wave buoys used for validation of the model data



(SPM) budget are wind-generated surface waves, the influence of which might have been underestimated in the past, and storm surges, which may export large amounts of sediment out of the tidal basins to the North Sea (Bartholdy and Anthony 1998).

Wind-generated surface gravity waves can influence SPM dynamics and fluxes on continental shelves and tidal flat systems. Due to an enhanced bottom shear stress during repeated cycles, waves significantly contribute to the erosion of sediments in coastal zones and over tidal flats. Once suspended, SPM can be transported by wind-driven, density-driven, or tide-induced currents to other locations. The study of Santamarina Cuneo and Flemming (2000) gives observational evidence of the importance of waves. They measured the import and export of SPM through the tidal inlet between two barrier islands located in the southern North Sea. In the presence of enhanced wind-generated surface waves, a net import of sediment into the tidal basin was observed. This net import was explained by an increased erosion of sediments in front of the barrier islands, where high waves from the North Sea reach the coasts of the islands. Once suspended, sediments are transported into the tidal basin by inward-flowing tidal currents.

Other field studies (see, e.g., Bassoullet et al. 2000) and modeling studies of different model complexity have demonstrated the influence and significance of

wave effects on the sedimentary system of coasts and continental shelves (see, e.g., Blaas et al. 2007; Condie and Sherwood 2006; Liang et al. 2007; Roberts et al. 2000).

Storm surges also significantly influence the sediment budget of tidal flat systems. During these events, the bottom shear stress is enhanced due to increased current speeds and dramatically increased wave activity. Bartholdy and Anthony (1998) investigated the sediment budget of a tidal system in the Danish Wadden Sea and demonstrated the importance of storm activity to export fine sediments from the tidal flat system towards the open ocean (North Sea). This impact of storms and storm-generated surface waves was also demonstrated by Warner et al. (2008) for sediment dynamics in Massachusetts Bay, USA, using the *Regional Ocean Modeling System* (ROMS).

A first attempt to investigate the influence of wind-generated surface gravity waves on suspended sediment dynamics in the study area was performed by Stanev et al. (2006). They used a simple analytical wave parameterization based on a formulation of Roberts et al. (2000), which accounted for wave breaking and which related wave-induced bottom shear stress to significant wave height. With this parameterization, Stanev et al. (2006) generated realistic dynamical features for suspended sediments. However, this parameterization did not account for growing or shoaling of waves near

the coast, which might lead to increased bottom shear stresses close to the shoreline.

The aim of this modeling study is to better understand the influences of storm surges and wind-generated surface waves on SPM dynamics in the East Frisian Wadden Sea. In order to increase the realism of the numerical model, the simple wave shear stress approach of Stanev et al. (2006) was extended by modeling the generation and dissipation of wind-generated surface waves with the third-generation wave model SWAN (Simulating Waves Nearshore) of Booij et al. (1999). The numerical modeling system is completed by the hydrodynamical General Estuarine Transport Model (GETM) (of Burchard and Bolding 2002) and a SPM module attached to the GETM.

With this modeling system, the wave and sediment dynamics during two ship cruises, one in October 2007 and the other in February 2008, was modeled for validation purposes. Furthermore, different scenarios with artificial wind forcing and tide-driven sea surface elevation with and without wind-enhanced sea level were considered. Finally, the effect of storm *Britta*, which was one of the most severe storm events in the North Sea region in the last hundred years, on sediment dynamic was simulated.

2 The study site

The study site (see Fig. 1c) is part of the East Frisian Wadden Sea, which is located in the southern part of the North Sea along the northwest coast of Germany. It consists of several barrier islands and tidal basins with large tidal flats between the islands and the mainland coast. The tidal basins are connected via tidal inlets with the North Sea.

2.1 Hydrodynamics

The tidal amplitude in this area is about 1.5 m during spring tides and about 1.0 m during neap tides. This places the tidal variability in the upper meso-tidal range. Figure 2 displays a time series of surface water level showing the spring to neap tide variability near the island of Spiekeroog in August 2007.

Under normal weather conditions, tidal current velocities can reach values of up to 1.5 m/s in these inlets and up to 0.3 m/s on the tidal flats (see, e.g., Chang et al. 2006; Santamarina Cuneo and Flemming 2000; Stanev et al. 2003). During one tidal period, water exchange between the North Sea and individual back-barrier basins through the tidal inlets varies from 40 to 170 · 10⁶ m³ according to model simulations of Stanev

et al. (2003). These variations in tidal prisms deviate to some extent from the simple product of the tidal range and the mean areas of the different tidal basins because the flooded areas of the tidal basins change in the course of a tidal cycle (Stanev et al. 2003b).

2.2 Wind and wave climatology

The North Sea is located in the northern hemisphere latitudinal belt of the atmospheric westerlies. Therefore, winds predominantly come from westerly directions, and according to the Nordsee Report of the *Federal Maritime and Hydrographic Agency* (BSH) (Loewe et al. 2006), this was the case for 65% of the North Sea winds in 2003, and even for 75% in 2004. In 2004 (which was a normal year concerning wind statistics), mean wind speeds ranged from about 7 m/s (4 Bft) in the summer season to about 10 m/s (5–6 Bft) in the autumn season (Loewe et al. 2006).

To quantify the wave climatology at the study site, Fig. 3 shows joint distributions of significant wave height and peak period at the FINO wave buoy in the North Sea and at the time-series station in the back-barrier tidal channel close to the island of Spiekeroog. The joint distribution was defined by:

$$JD(H_{sig}, T_{peak}) = \frac{\text{number in spec. bin}(H_{sig}, T_{peak})}{\text{total number of measurements}} \cdot 100 \tag{1}$$

The FINO data cover the period from January 2006 to August 2007 and show a dominant wave height of about 1.25 m. Behind the islands at the time-series

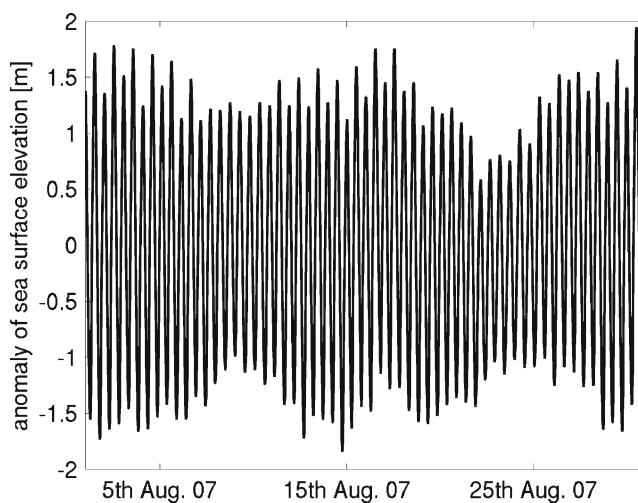


Fig. 2 Anomalies of sea surface elevation at the time series station near the island of Spiekeroog in August 2007 (for the position of the time-series station, see Fig. 1)

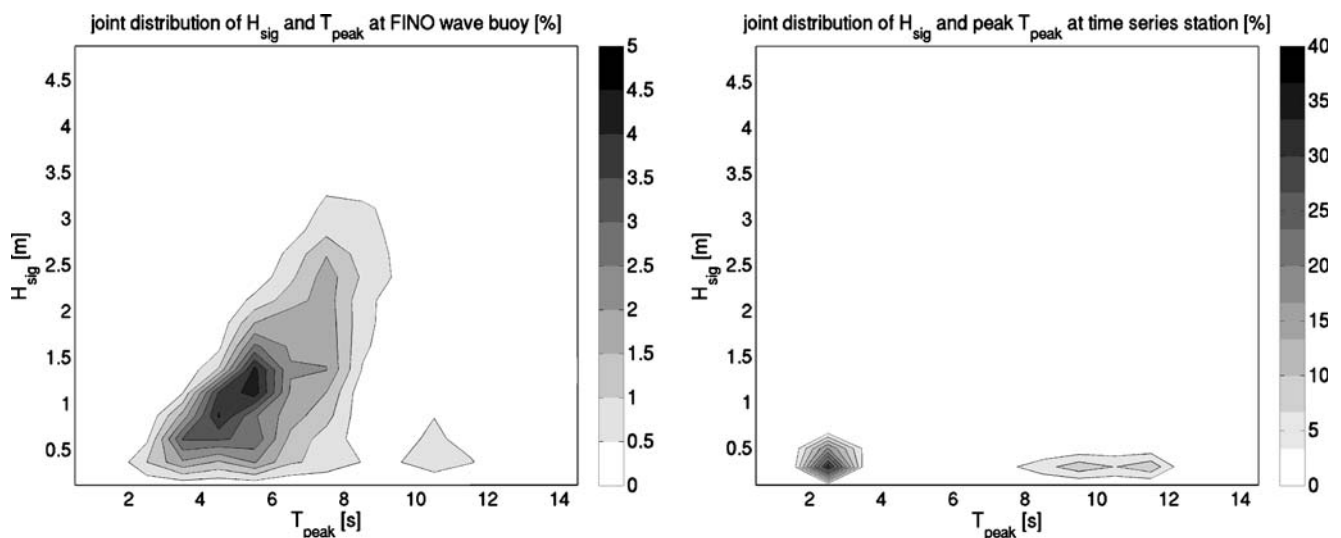


Fig. 3 Joint distribution (defined in Eq. 1) of significant wave height (H_{sig}) and peak period (T_{peak}) at the FINO wave buoy (*left*) and the time-series station (*right*). The FINO data were measured during January 2006 and July 2007 and are binned with $\Delta H_{\text{sig}} = 0.25 \text{ m}$ and $\Delta T_{\text{peak}} = 1 \text{ s}$, with a total number of

11,797 measurements. Wave data at the time series station cover a period from December 2006 to June 2007 and are binned with $\Delta H_{\text{sig}} = 0.20 \text{ m}$ and $\Delta T_{\text{peak}} = 1 \text{ s}$, with a total of 2,201 measurements. Note the different gray shading scales of the two figures

station (period between December 2006 and June 2007), the significant wave height decreases to about 0.35 m. These data demonstrate the protective influence of the barrier islands for the tidal flats against the incoming waves from the North Sea.

These results are consistent with wave observations reported by Krögel and Flemming (1998), who estimated wave heights between the island of Langeoog and the main coast. According to their study, in the winter season with their stronger winds, significant wave heights can exceed 0.8 m, whereas in the calmer summer season, wave heights barely reach 0.4 m. Therefore, due to increased wave heights, winter seasons will be more effective in eroding sediments than summer seasons.

2.3 Sedimentary system and observed SPM fluxes

The size distribution of the sedimentary system ranges from fine-grained muddy sediments with diameters $\leq 63 \mu\text{m}$ to medium sands with mean grain sizes around $300 \mu\text{m}$. Several authors have documented that the intertidal sediments in that region are arranged in well-defined shore-parallel belts showing a general shoreward fining trend (see top left panel in Fig. 13 and, e.g., Flemming and Nyandwi 1994; Flemming and Ziegler 1995). Besides muddy areas along the mainland coasts, sand flats with mud contents below 2% dry weight, e.g., the *Swinnplate* south of the island of Spiekeroog, are common.

To get an impression of the amount of SPM transported in the water column through the tidal inlets, measurements of Santamarina Cuneo and Flemming (2000) based on ADCP data are referred to. They found that, under fair-weather conditions [wind speeds below 6.0 m/s (4 Bft)], maximum concentrations of suspended matter were relatively low (about 60 mg/l), with no significant net import or export. Under windier conditions [wind speeds about 10 m/s (5–6 Bft)], measured SPM concentrations increased to 130 mg/l. In this case, a net import of sediment of up to 2,950 tons into the tidal basin was estimated over one tidal cycle, of which 1,640 tons was contributed by the sand fraction and 1,310 tons by the mud fraction (Santamarina Cuneo and Flemming 2000).

In order to quantify the effect of currents and waves on the sedimentary system, the critical shear stress, which must be overcome to erode the sediment, is important. Austen and Witte (2000) measured the critical bottom shear stress for sediments at a study site close to the island of Baltrum. Their measured values vary from 0.15 to 1.0 N/m² for muddy and sandy sediments, respectively. These values agree with the critical shear stresses used in this modeling study.

3 Model description

The numerical experiments were based on a coupled system of models comprising a hydrodynamic core

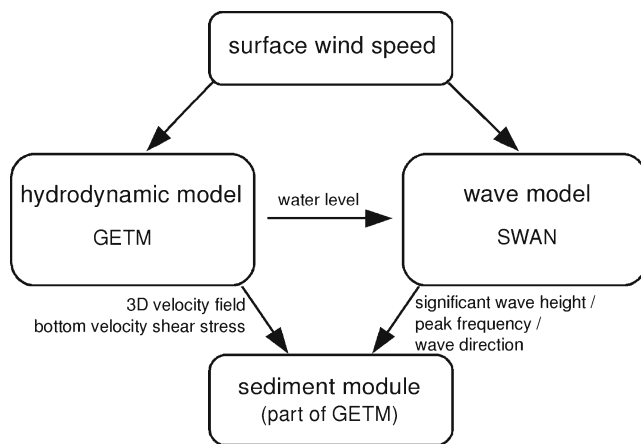


Fig. 4 Coupling of the hydrodynamic model (GETM) with the wave model (SWAN)

model, a wave model, and a SPM module attached to the hydrodynamical core model (see Fig. 4). The models are briefly described in the next subsections with references to more detailed discussions in the literature where appropriate.

3.1 Hydrodynamic core model

The hydrodynamic computations were performed with GETM, the General Estuarine Transport Model (Burchard and Bolding 2002). A recent model documentation is given by Burchard et al. (2007).

GETM is a prognostic three-dimensional hydrodynamical model especially suited for shallow coastal regions under the influence of tidal currents where substantial areas are prone to drying and flooding during a normal tidal cycle. The model is based on the horizontal momentum equations and the continuity equation with two prognostic equations for the turbulent kinetic energy and its dissipation rate influencing the vertical eddy viscosity coefficient. In horizontal directions, GETM uses a constant momentum diffusivity (viscosity, A_m), and in order to increase numerical stability, GETM provides a constant horizontal diffusivity, A_n , to smooth surface elevation. This hydrodynamic core model has been applied and validated in various recent studies (see, e.g., Burchard et al. 2004; Stanev et al. 2003, 2006, 2007).

As mentioned before, this study is concerned with the effects of storms on the sedimentary system. To account for the effect of increased ocean surface roughness due to higher waves during storms, a wind-speed-dependent drag coefficient C_D was implemented to calculate the surface wind stress from wind speeds. The

following formula provided by Holthuijsen (2007) was taken:

$$C_D = \begin{cases} 1.2875 \cdot 10^{-3} & \text{for } U_{10} < 7.5 \text{ m/s} \\ (0.8 + 0.065 U_{10}) \cdot 10^{-3} & \text{for } U_{10} \geq 7.5 \text{ m/s} \end{cases} \quad (2)$$

Here, U_{10} denotes the wind speed at a 10-m height above the sea surface.

3.2 Wave model

Surface gravity wave propagation and generation by atmospheric winds were simulated with the two-dimensional wave model SWAN (Booij et al. 1999). SWAN was operated in nonstationary mode using its default methods and parameter values to model wave growth, wave propagation, and dissipation. In detail, the processes of wave generation, quadruplet wave-wave interactions, white capping, bottom friction, depth-induced breaking, and triad wave-wave interactions were activated. In coastal waters, the processes of wave reflection and diffraction were neglected.

The waves in the East Frisian Wadden Sea during the two ship cruises and the real storm surge event were modeled using a one-way nested system of different model domains with increasing spatial resolution. The largest area with the coarsest resolution of 20-km grid spacing covers the whole North Atlantic. This enlarged area was needed to determine the wind-generated waves in the Atlantic, which would reach the North Sea, e.g., in the form of swell.

Embedded into this large domain was a model domain of the North Sea area (see blue box in Fig. 1a) with a 5-km grid resolution. The wave boundary conditions for this model domain were obtained from the Atlantic domain. Finally, the third nested domain covered the area of the German Bight with a resolution of 2 km (see green box in Fig. 1a). From this third model area, the wave boundary conditions were obtained for the wave simulations in the Wadden Sea with a grid resolution of 200 m. As time step for nonstationary computations, 60 min was taken for the large Atlantic domain, 30 min for the North Sea and the German Bight domain, and 15 min for the Wadden Sea model domain.

3.3 SPM module

Coupled to GETM was a SPM module (see Fig. 4), which was based on a diffusion–advection equation with an additional settling velocity. Five noncohesive

sediment fractions with diameters between 40 and 200 μm were considered. This module accounted for suspended sediment concentrations in the water column and the amount of sediment fractions at the bottom (which are termed bottom sediment pools in the following). Sediments were eroded from the bottom once a critical bottom shear stress was exceeded, and sediments were deposited when the bottom shear stress was below a critical value. The current-induced bottom shear stress was obtained from the hydrodynamic core model, GETM, and was calculated via an iterative procedure using a prescribed bottom roughness length z_0 . This bottom roughness length was set constant over the whole model domain and did not change during the model integration.

In addition to the bottom shear stress produced by the current field, sediments are also eroded by wave-induced shear stresses. These wave-induced bottom shear stresses were calculated in this study on the basis of a parameterization proposed by Soulsby (1997), which employed the wave field parameters delivered by SWAN. This wave shear stress parameterization was also used by Pleskachevsky et al. (2005) and Gayer et al. (2006) to study sediment dynamics in the North Sea. More details about the sediment module are presented in the [Appendix](#).

3.4 Coupling of modeling system components

The interaction of the different modeling system components is described in Fig. 4. The sediment module was part of the GETM model and received horizontal and vertical velocities from the hydrodynamical component of GETM. Wave parameters for calculating the wave-induced bottom shear stress were delivered by the wave model SWAN.

The wave model SWAN was operated in a nonstationary mode and was coupled to GETM in a very simple way. GETM delivered only the horizontal surface elevation to SWAN when the modeling system was used in coastal areas (in the Wadden Sea). In the case of the deeper North Sea or the Atlantic Ocean, SWAN was used in a stand-alone mode and was forced only by the wind field. In general, the wave model SWAN can also be forced by current speeds from the hydrodynamic component in addition to prescribing sea surface elevation. This may be important in the tidal inlets of the Wadden Sea region, where strong tidal currents can change the incoming wave field (Doppler shift in frequency, energy bunching changing the amplitude of the waves). Although possible, we decided not to include current speeds for calculating the wave field parameters with SWAN, as we encountered some

problems in matching observed wave parameters when we included the current speeds. Here, future tests are needed to identify and eliminate the reasons for these problems.

In the other direction, GETM did not see the wave fields calculated by SWAN, as we did not include wave-induced effects like radiation-stresses, which could influence current speeds. This interaction will be implemented in the future.

3.5 Model topography and surface wind forcing

The model topography for the Wadden Sea domain was generated from high-resolution bathymetric data provided by the German BSH (Hamburg and Rostock) and from the *Niedersächsischer Landesbetrieb für Wasserwirtschaft, Küsten- und Naturschutz* (NLWKN, Norden). The topography data for the large model domains used for wave modeling were taken from the ETOPO2 (2006) data set.

The wind velocities were obtained from several sources. For the large model domains of the Atlantic Ocean and the whole North Sea, NCEP reanalysis data provided by the NOAA/OAR/ESRL PSD, Boulder, CO, USA (Kalnay et al. 1996), were taken. For the local modeling of waves and currents during the two ship cruises, wind speeds from the time-series station in the Wadden Sea were used.

In the case of the storm Britta, we found that the temporal and spatial resolution of the NCEP data were not sufficient to match the observed wave or current velocity conditions. Therefore, wind data with a higher temporal and spatial resolution were taken from the German Weather Service (DWD) for the North Sea and the Wadden Sea. For modeling of waves in the Atlantic Ocean during storm Britta, we used NCEP data for the forcing, as data with a higher temporal and spatial resolution were not at our disposal.

3.6 Surface elevation at open boundaries

The hydrodynamical model, GETM, needs boundary conditions for the surface elevation at the open boundaries. For the simulation of the time periods of the two ship cruises in October 2007 and February 2008, sea surface elevation at the open boundaries was constructed from the measured surface elevation data at the time-series station. These data were extrapolated to the open western, northern, and eastern boundary points with a time shift from west to east to account for the travelling of the tidal surface Kelvin wave along the coasts of the North Sea.

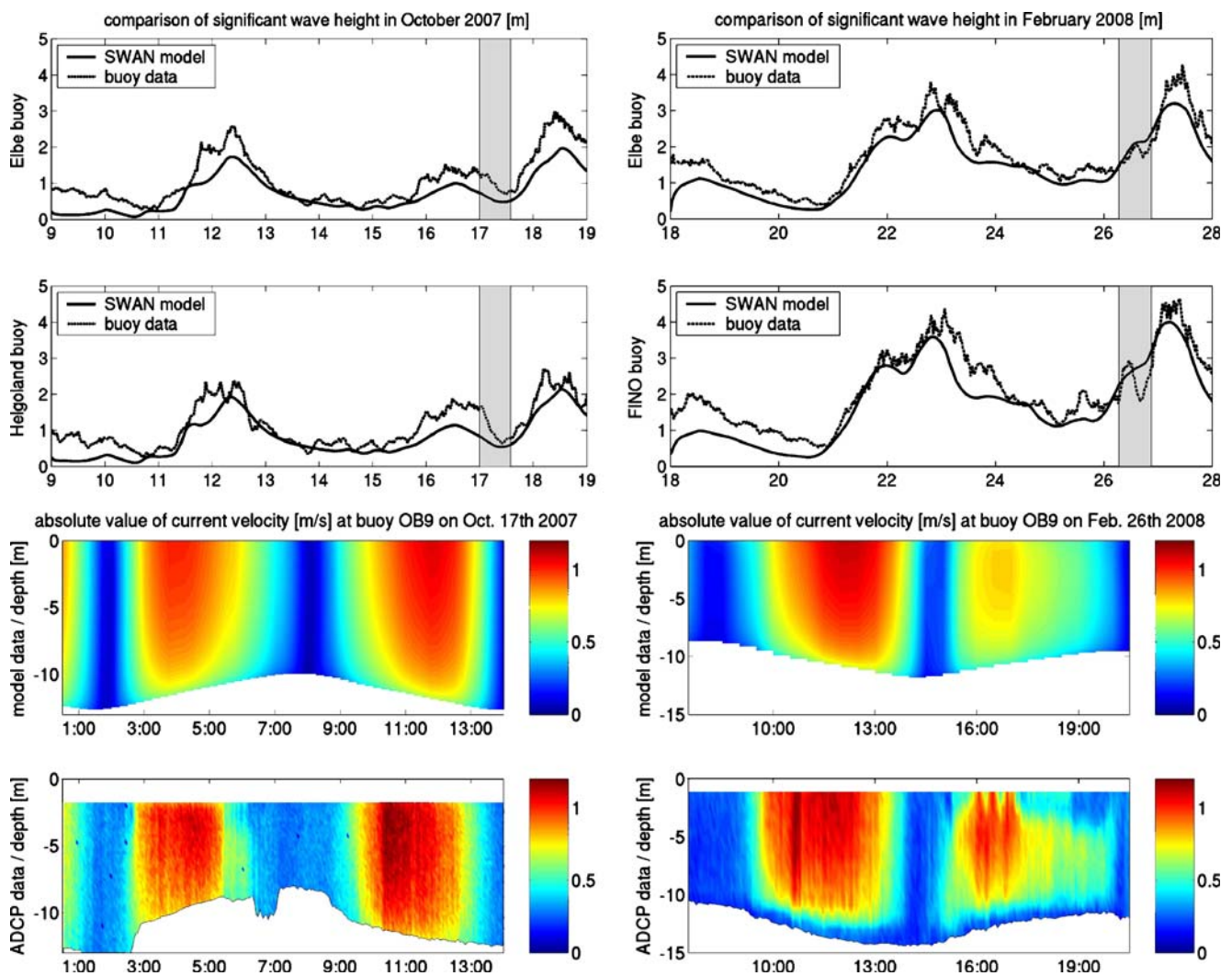


Fig. 5 Top row: Comparison of significant wave height (m) in October 2007 and February 2008 at the positions of the wave buoys (Elbe, Helgoland, and FINO) in the German Bight. The gray shaded areas denote the time interval where measurements of SPM concentrations and current velocities are available from the two ship cruises in the Wadden Sea. Bottom row: Time-depth

plots of measured and modeled current velocity (m/s) at the location of buoy OB9 (the approximate location of the anchored ship) in the tidal inlet between the islands of Langeoog and Spiekeroog. The left figure shows the situation in October 2007, the right one in February 2008

This procedure was also used to provide the surface elevation for the scenarios with artificial forcing functions. In this case, the artificial water level of the M_2 -tide or an artificial storm-surge water level was prescribed at the open boundaries with a time lag to account for Kelvin wave propagation.

For the numerical simulations of storm Britta, the sea-level boundary data were extracted from an external modeling system operated by Joanna Staneva (Staneva et al. 2008). With this modeling system, sea surface elevation was modeled for the whole area of the German Bight on the basis of realistic surface wind speeds and atmospheric pressure conditions.

4 Model validation experiments

The numerical modeling system was validated by comparing modeled and measured concentrations of SPM and current velocities obtained by the two ship cruises with the research vessel “FK Senckenberg” in October 2007 and February 2008. During these cruises, vertical profiles of current velocity were measured with a hull-mounted ADCP at a particular position in the tidal inlet between the islands of Langeoog and Spiekeroog (at buoy OB9, $53^{\circ}44.87'/7^{\circ}40.30'$, i.e., close to the time-series station, see Fig. 1). Furthermore, suspended sediment content at about 1.5 m below the sea surface was

obtained from water samples and filtering. In addition, vertical profiles of SPM were estimated via an optical method, which is described in more detail in Badewien et al. (2009). On the basis of these observations, some free model parameters of the sediment and the hydrodynamic module were slightly changed. These parameters were then used in hindcasting storm Britta and for the idealized test cases.

Unfortunately, the wave measurement system at the time-series station was out of order during these cruises. Therefore, the modeled wave heights in the Wadden Sea region could not be validated. Instead, wave data recorded by wave buoys in the German Bight (see Fig. 1) were taken and compared with the modeled wave heights obtained from SWAN.

During these cruises, weather conditions were calm in October 2007 and windy in February 2008. This can also be seen from Fig. 5, where the measured and modeled wave heights at the German Bight wave buoys during these cruises are depicted. Whereas the significant wave height was around 1 m in October 2007, it was between 1.5 and 2.5 m in February 2008. This is an indication that wave effects in the East Frisian Wadden Sea were more dominant during the cruise in February 2008 compared to that in October 2007.

Figure 5 demonstrates that the model captures wave heights and current velocities during the cruises in the right order of magnitude. Concerning wave heights, the observed high-frequency variability in the order of

several hours is not reproduced. The reason for this might be the used NCEP wind data with their coarser temporal resolution of 6 h. The modeled fluid velocities are in the right order as well. However, the maxima of current velocity are underestimated, especially during falling water. This might lead to an underestimation of the exported amount of sediment out of the tidal basin to the North Sea.

Figure 6 shows modeled and measured SPM concentrations during the cruises in October 2007 and February 2008. As can be seen from these graphs, the modeled SPM concentrations are of the right order of magnitude. However, in October the sediment concentrations are somewhat overestimated, especially at the start of the time series for October 2007. In February 2008, for the situation with stronger winds, SPM concentrations compare very well in magnitude and timing (phase) with the observations during flood (rising water), whereas for ebb (falling water, the second peak), the model underestimates the sediment concentration.

In any case, the dashed blue curve in Fig. 6, which shows the model results with no wave activity allowed in the SPM module, demonstrates clearly the importance of considering waves in SPM dynamics of the East Frisian Wadden Sea. Without wave activity in the SPM module, the magnitude of the SPM concentration is dramatically underestimated.

In comparison to the measurements, the model underestimates current velocities during the falling

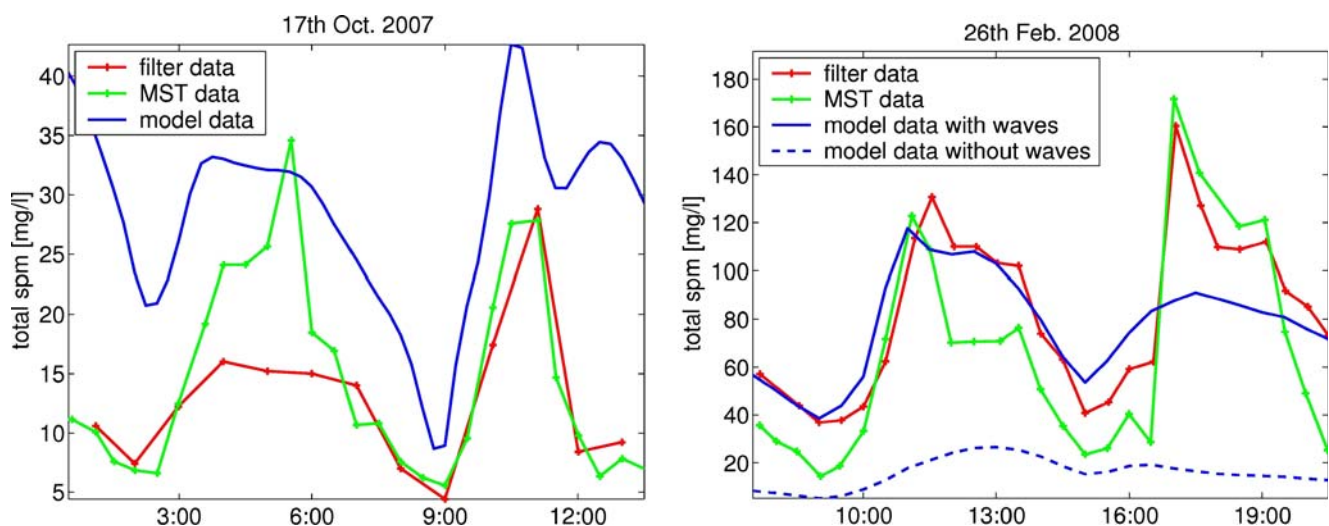


Fig. 6 Measured and modeled suspended sediment concentrations 1.5 m below the water surface at a fixed position in the tidal inlet between the islands of Langeoog and Spiekeroog (position of buoy OB9). The figure on the left shows the situation on 17 October 2007 with calm winds, the figure on the right on 26 February 2008 with stronger winds (note the difference in scale

for the SPM concentrations). The green and the red curves denote concentrations measured by two different methods. The blue curves denote model results. In addition, the lowest dashed blue curve in the right-hand figure denotes the model result with wave action switched off

tide. This may be due to the fact that the external forcing parameters are rather crude and the model resolution is low. In the case of SPM, these spot measurements may not be representative for the respective model domain.

As demonstrated, the modeling system had some problems in matching current velocities and SPM concentrations during the ship cruise on the 26th of February 2008. To test whether the modeling system at least captures the right order of magnitude and direction of SPM transport, the measured and modeled SPM concentrations were multiplied with the measured and modeled current velocities at 1.5-m water depth at the measurement position in the tidal channel between the islands of Langeoog and Spiekeroog. In the period between 8:30 a.m. and 8:30 p.m., there was an observed net import of SPM into the tidal basin in the order of 1,200 kg/m². The numerical model produced a net import of 590 kg/m². Although the absolute values deviate by a factor of two, the modeling system got at least the right direction of sediment transport for this specific location and time period.

In Table 1, the selected model parameters and resolutions are presented. As mentioned above, for the SWAN wave model, default parameter values of the different processes of wave generation and dissipation were taken from the standard set of parameters provided in the SWAN manual.

5 Idealized test cases

Numerical models are unique in that they allow changes in the values of certain physical parameters to study the effects of different forcings or, indeed, to simulate situations without such forcings. In order to discriminate between the effects of various physical influences on circulation and SPM transport, tests with artificial forcing functions were conducted in which different combinations of surface elevation (water depth), wind speeds, and wave parameters were considered.

In these five artificial scenarios (see Table 2), normal weather conditions are characterized by a prescribed surface elevation at the open boundaries dominated by

Table 1 Model parameters used for the hydrodynamic core model GETM, the wave model SWAN, and the SPM module

GETM	
Grid resolution, $\Delta x = \Delta y$ (m)	200
Horizontal viscosity A_m (m ² /s)	1.0
Horizontal numerical sea-surface elevation diffusivity A_n (m ² /s)	1.0
Vertical background viscosity (m ² /s)	$1.0 \cdot 10^{-6}$
Constant bottom roughness length z_0 (m)	0.001
Critical depth (m)	0.5
Minimal depth (m)	0.1
SWAN	
Atlantic model domain	
Spatial grid size $\Delta x = \Delta y$ (km)	20
Logarithmically scaled frequency bins	50 / 0.02–1.0 (Hz)
Directional bins between 0° – 360°	24
Time step (min)	60
German Bight model domain	
Spatial grid size $\Delta x = \Delta y$ (km)	5
Logarithmically scaled frequency bins	50 / 0.02 – 1.0 (Hz)
Directional bins between 0° – 360°	24
Time step (min)	30
Wadden Sea model domain	
Spatial grid size $\Delta x = \Delta y$ (km)	0.2
Logarithmically scaled frequency bins	50 / 0.02 – 1.0 (Hz)
Directional bins between 0° – 360°	24
Time step (min)	15
SPM module	
Sediment density ρ_S (kg/m ³)	2650
Erosion constant M_e [kg/(m ² s)]	$2.5 \cdot 10^{-4}$
Vertical background diffusivity A^b_v (m ² /s)	$1.0 \cdot 10^{-6}$
Constant horizontal diffusivity A_h (m ² /s)	$1.0 \cdot 10^{-3}$
Constant water temperature, artificial cases (°C)	4
Constant water temperature, storm Britta (°C)	8

Table 2 Overview over the different idealized scenarios and the corresponding forcing conditions

Scenario	Surface elevation	Wind speed / direction	Waves $H_{sig} / T_{peak} /$ direction
S1	M2	–	–
S2	M2	–	1.25 m / 5.5 s / SE
S3	M2	7.5 m/s / NW	1.25 m / 5.5 s / SE
S4	M2 + storm	storm	–
S5	M2 + storm	storm /NW	storm / SE

Surface elevation denotes the prescribed sea surface elevations at the open boundaries. Wind denotes the used wind speed and direction (coming from) in 10-m height. Finally, waves denotes the prescribed wave boundary conditions at the northern boundary with the meaning significant wave height H_{sig} / peak period T_{peak} / direction (going to). The boundary forcing functions of storm surge scenarios S4 and S5 are plotted in Fig. 7.

the M_2 tidal component with an amplitude of 1.25 m. Furthermore, if present (scenario S3), winds came from the northwest with a constant wind speed of 7.5 m/s.

For storm surge conditions, the water elevation is simulated by adding a Gaussian elevation peak to the M_2 tidal signal. Similarly, the normal wind speeds and wave parameters to simulate the effects of a storm surge are enhanced in the whole model domain. These forcing functions have realistic magnitudes, which can be seen in Fig. 7, where these artificial forcing functions are compared with the corresponding properties

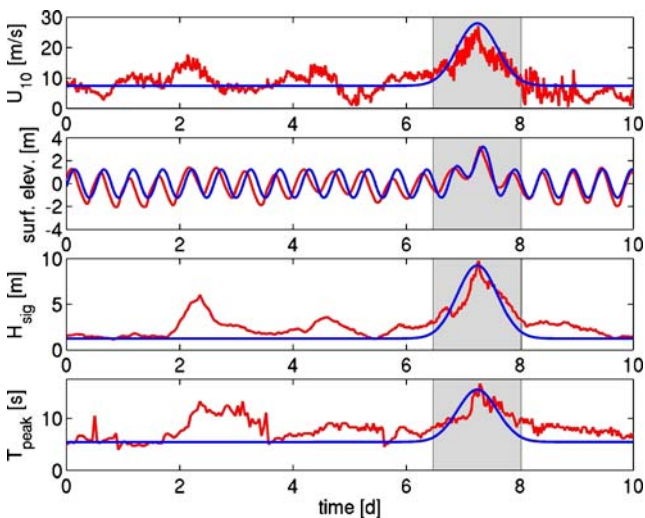


Fig. 7 Forcing functions for artificial storm-surge scenarios S4 and S5 (blue curves). To relate their magnitude to real data, the respective properties measured during storm Britta in November 2006 (red curves) were plotted. The anomaly of surface elevation and wind speed were recorded at the time-series station, and significant wave height and peak period were measured at the FINO wave buoy. The gray shaded areas denote the time interval T , which is identified with the storm-surge period

measured during storm Britta in 2006. The anomaly of sea-surface elevation and wind speed presented in this figure were recorded at the time-series station close to the island of Spiekeroog and significant wave height and peak period were measured at the FINO wave buoy (see Fig. 1).

To model the wave influence for normal and stormy weather conditions, the wave spectrum at the northern boundary of the Wadden Sea model domain was prescribed. For the moderate weather scenarios S2 and S3, a stationary JONSWAP spectrum with the parameters presented in Table 2 was used. For the storm surge scenario S5, the prescribed JONSWAP spectrum was changed to account for different peak period and significant wave height according to the functions presented in Fig. 7; only wave direction was held constant. If wind was present in scenarios as S3 and S5, waves were additionally generated in the model domain via linear growth according to equations by Cavaleri and Malanotte-Rizzoli (1981) already implemented in SWAN. Once present, waves could grow further according to Komen et al. (1984).

The sediment pools at the sea floor were initialized with a uniform distribution over the whole model domain. The initial amount of sediment for each fraction (100 kg/m^2) was chosen to assure that there would be no lack of sediment in any bottom grid cell during the model integration.

5.1 Erosion potential

The five scenarios mentioned above have different ways to potentially erode sediment. To estimate the effectiveness of sediment erosion under different physical forcing conditions, a parameter K_{ero} is defined as follows:

$$K_{ero} := \frac{1}{T} \int_0^T M_c(\tau_B, \tau_c) dt \tag{3}$$

$$M_c := \begin{cases} \frac{(\tau_B - \tau_c)}{\tau_c} & \text{if } \tau_B > \tau_c \\ 0 & \text{if } \tau_B < \tau_c \end{cases}$$

Here, τ_B denotes bottom shear stress, which is calculated from current velocity and wave conditions after Eq. 15 (see Appendix). Furthermore, τ_c denotes a critical bottom shear stress for which sediment erosion starts, and T denotes the time interval over which the erosion potential is measured. This parameter, K_{ero} , is high in regions where bottom shear stress is frequently above the critical value and low in regions with very low bottom shear stresses. For these numerical experiments, a value of $\tau_c = 0.15 \text{ N/m}^2$ was taken, which

corresponds to the critical shear stress of noncohesive sand with a grain size of 120 μm .

From the simulated wave climate and current velocities in the Wadden Sea model domain, the bottom shear stress, τ_B , was calculated using Eq. 15 for each scenario over a time interval T of three tidal cycles. This time interval is depicted as the gray shaded area in Fig. 7 and includes the storm surge conditions of the forcing functions.

In Fig. 8, this measure of erosion is shown for the five different scenarios. In the case with only the M_2 tide forcing (scenario S1), the potential of sediment erosion is mostly dominant in front of and in the tidal inlets between the barrier islands due to the high current speeds.

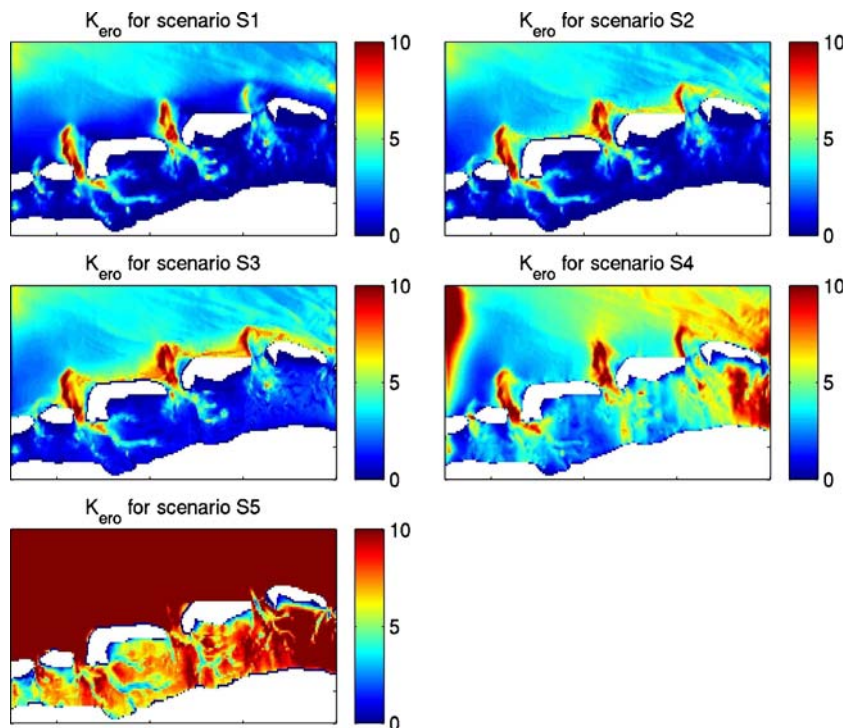
In scenario S2, only incoming waves from the North Sea are considered without any wave growth in the model domain. These incoming waves have an increased net effect on sediment erosion compared to scenario S1 in front of the barrier islands. Behind the islands, i.e., in the tidal basins, the waves are of small amplitude and do not contribute very much to sediment erosion. This situation changes somewhat if waves are also generated in the tidal basins by moderate winds from the northwest (scenario S3). In contrast to scenario S2, there is a small increase in sediment erosion on the tidal flats and a stronger increase of erosion in front of the barrier islands.

It is evident from scenarios S1 to S3 that, in the presence of moderate winds, the potential of erosion due to waves on the tidal flats is still much smaller than the potential of erosion in the tidal channels and tidal inlets due to the currents. However, in front of the barrier islands, moderate winds can lead to enhanced erosion of sediments via wind-generated surface gravity waves, which is of the same magnitude as the erosion due to tidal currents.

The storm surge scenarios with and without waves are discussed in the following. The situation of a storm surge with an additional surface elevation and enhanced wind speeds, but no waves (scenario S4), differs only from the other scenarios by enhanced erosion in the eastern part of the model domain. The reason for this might be a stronger eastward-flowing current component due to the increased wind stress in the tidal basins that are present in the whole tidal basin area. These enhanced currents have a stronger potential for sediment erosion than waves generated in the tidal basin region by moderate winds.

The situation changes drastically when wave effects are included (scenario S5). The waves lead to a huge erosion potential in front of the barrier islands, whereas the tidal flats are again protected to some extent by the barrier islands. However, there is also much stronger sediment erosion on the tidal flats compared to the case without waves (scenario S4).

Fig. 8 Measure of sediment erosion due to currents and wind-generated surface gravity waves according to Eq. 3 for the five artificial scenarios listed in Table 2



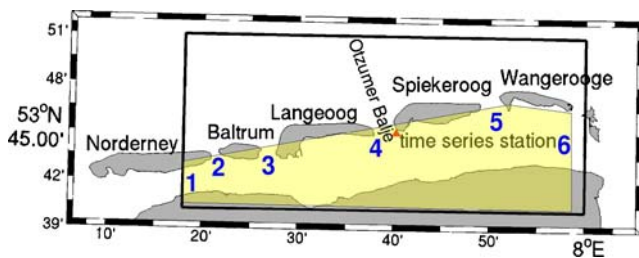


Fig. 9 The *yellow shading* denotes the area for which changes in bottom sediments due to the different scenarios over the time interval of three tidal cycles were calculated. Furthermore, the *blue numbers* denote the sections for which suspended sediment transports were determined

From scenarios S4 and S5, it is also evident that the modeling system suffers to a certain degree from somewhat artificial and unrealistic boundary conditions. At the western and eastern model boundaries, the calculated sediment erosion rates are clearly too high. One reason for this might be the way the sea-surface elevation boundary conditions were prescribed. To overcome these problems, the open boundaries will be placed at a greater distance from the area of interest in future studies. In addition, for scenario S5, there appears to be a progressive increase in erosion potential from west to east behind the barrier islands. This trend might be due to the procedure of calculating wind-generated surface gravity waves. In this scenario (S5), the winds dominantly came from the west. It therefore seems likely that, in the western parts of the model domain, the generation of waves is fetch-limited, whereas the waves might be fully developed in the eastern part of the model domain. Again, this problem may be solved by shifting the model boundaries to more remote locations.

In summary, one can conclude from the considered potential of sediment erosion that tidal currents are very effective in eroding sediments during normal weather conditions with low to moderate wind speeds (scenarios S1–S3). The main areas of erosion are situated in front of the tidal inlets and in the tidal channels. Waves play a definite role in front of the barrier islands where they have an erosion potential similar to that of the tidal currents. However, on the tidal flats, waves are not very important for sediment erosion if wind speeds are small. It will be demonstrated below that this additional erosion due to waves in front of the barrier islands under moderate wind speeds leads to an enhanced import of sediment into the tidal basins. During storm-surge conditions, waves become increasingly dominant in the Wadden Sea region.

5.2 Budgets of SPM

In this section, patterns of sediment erosion/deposition on the tidal flats and sediment transport from the North Sea into the tidal basins and vice versa are presented. The yellow area in Fig. 9 denotes the region for which net sediment changes were determined for each of the five scenarios over the time interval of three tidal cycles, which includes the storm surge conditions for scenarios S4 and S5. In addition, the four inlets (2–5) and the open boundaries along the western (1) and eastern (6) model domain are shown for further reference.

The cumulative transport of suspended sediment across any of the six sections depicted in Fig. 9 was calculated as follows, where A and B represent the end points of each section:

$$T_{\text{cum}}(t) = \int_0^t \int_A^B \int_{-h}^{\zeta} \text{SPM}(t', s, z) \cdot v_{\perp}(t', s, z) dz ds dt' \quad (4)$$

SPM denotes SPM concentration along that section, v_{\perp} the velocity perpendicular to the section, s the horizontal coordinate along that considered section between the end points A and B, and z the water depth.

The cumulative transport $T_{\text{cum}}(t)$ across section 4 (between the islands of Langeoog and Spiekeroog) for scenario S1 (tidal forcing only) is shown in Fig. 10. This figure clearly illustrates that all sediment fractions show a net import into the tidal system through this inlet. The largest variability is observed for the smallest sediment fraction. The gray shaded area in this figure denotes

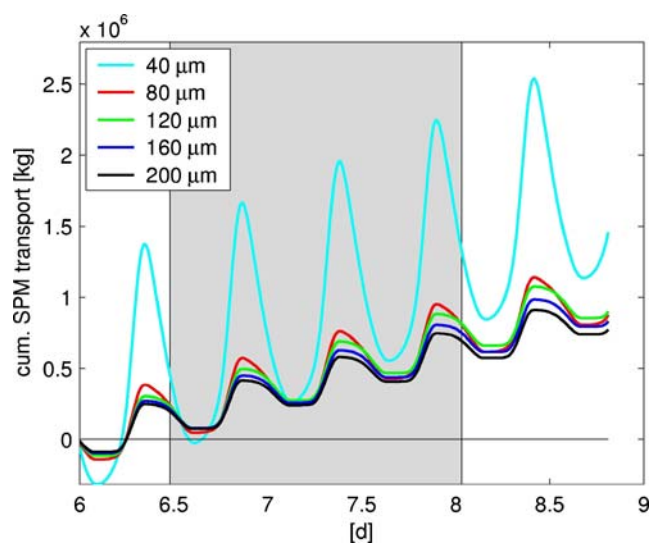


Fig. 10 This figure shows the cumulative SPM transport through the Oztumer Balje tidal inlet (section 4) for scenario S1 calculated on the basis of Eq. 4

the time interval of the three tidal cycles for which the net sediment transports through all inlets and bottom sediment change in the tidal basins were calculated.

A different view of the relationships between import and export of SPM through the inlets and open boundaries to the west and east is given in Fig. 11. In the case of the normal weather scenario, S1, it is evident that there is a substantial net import of SPM into the tidal basins in the case of inlets 3 and 4, but small net exports through inlets 2 and 5 as well as across the open boundaries 1 and 6. This net import of SPM results in an accumulation of bottom sediments for all sediment fractions in the Wadden Sea, as can be seen in Fig. 12.

When waves are added to the tidal forcing (scenario S2), the SPM import into the tidal basin area increases significantly (see Fig. 11). The net import through the Otzumer Balje (section 4) over one tidal cycle is about 10,000 tons for scenario S2 and 1,000 tons for scenario S1 (the values in Fig. 11 are valid for three tidal cycles). For scenario S2, the modeled value is three times larger than the measured value of 2,950 tons provided by Santamarina Cuneo and Flemming (2000). However, for scenario S1, the modeled value is three times smaller, which demonstrates that our modeling system can actually reproduce the observed transport of

Santamarina Cuneo and Flemming (2000) by tuning the considered wave spectrum at the northern boundary.

Even if the net import of SPM for scenario S2 seems to be overestimated with respect to measured values, the comparison between scenario S1 and S2 demonstrates that the mechanism proposed by Santamarina Cuneo and Flemming (2000), namely that sediment erosion due to waves in front of the barrier islands should lead to an enhanced import of suspended sediment into the tidal basins, is correct.

Comparing scenarios S2 and S3, it is evident from Fig. 12 that there is a net accumulation of sediment in the tidal basin area for both scenarios. However, in the case of scenario S3, where additional westerly winds generate surface gravity waves over the tidal flats and a net eastward current, the accumulation of the finest sediment fraction is reduced compared to the coarser sediment fractions. This can be explained by the stronger erosion of the finest sediment fraction by wave action and the longer suspension times in the water column. Therefore, the accumulation of finer sediment fractions is reduced relative to the coarser sediment fractions, which results in a net reduction of fine sediments in the tidal basin area. In summary, stronger surface waves over the tidal flats and a particular net

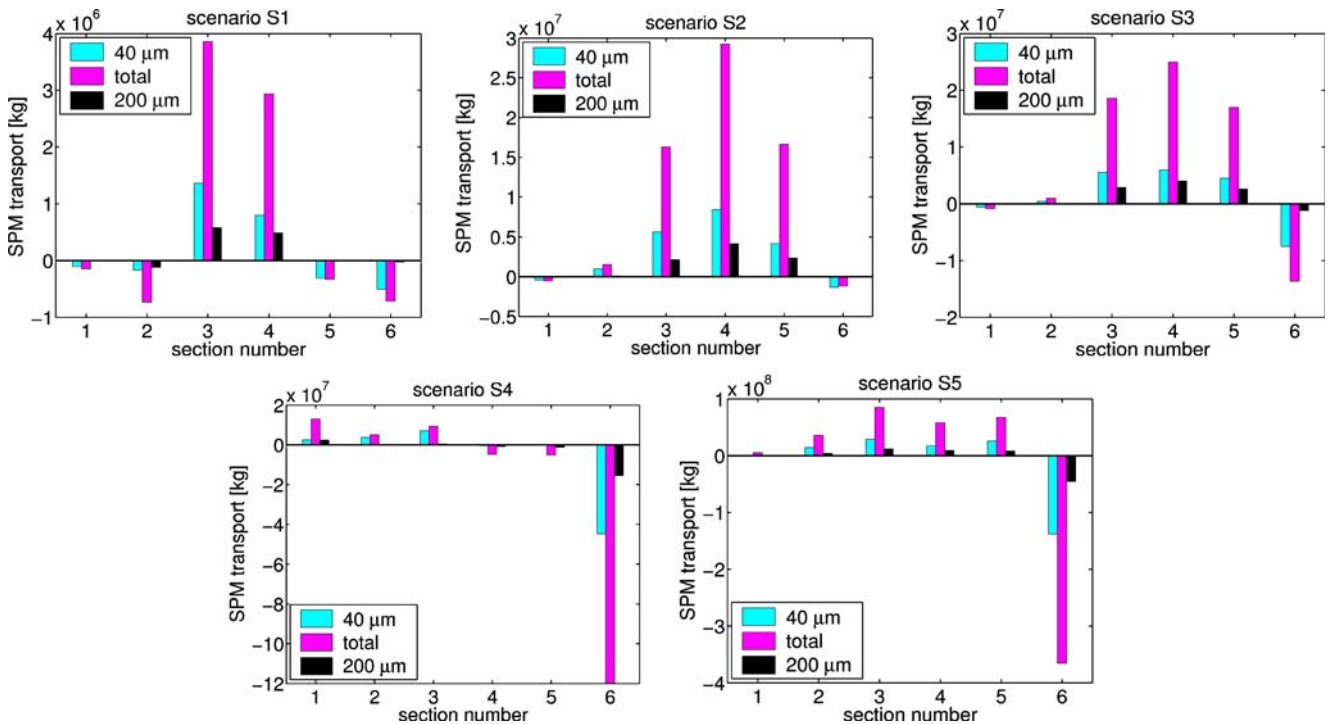


Fig. 11 Suspended sediment transports through all openings (1–6) to the back-barrier tidal flat system for the five different artificial scenarios. The transports were calculated over three tidal

cycles, which correspond to the storm surge period for scenarios S4 and S5. Positive values denote an import of sediment into the tidal basin area (yellow shading in Fig. 9)

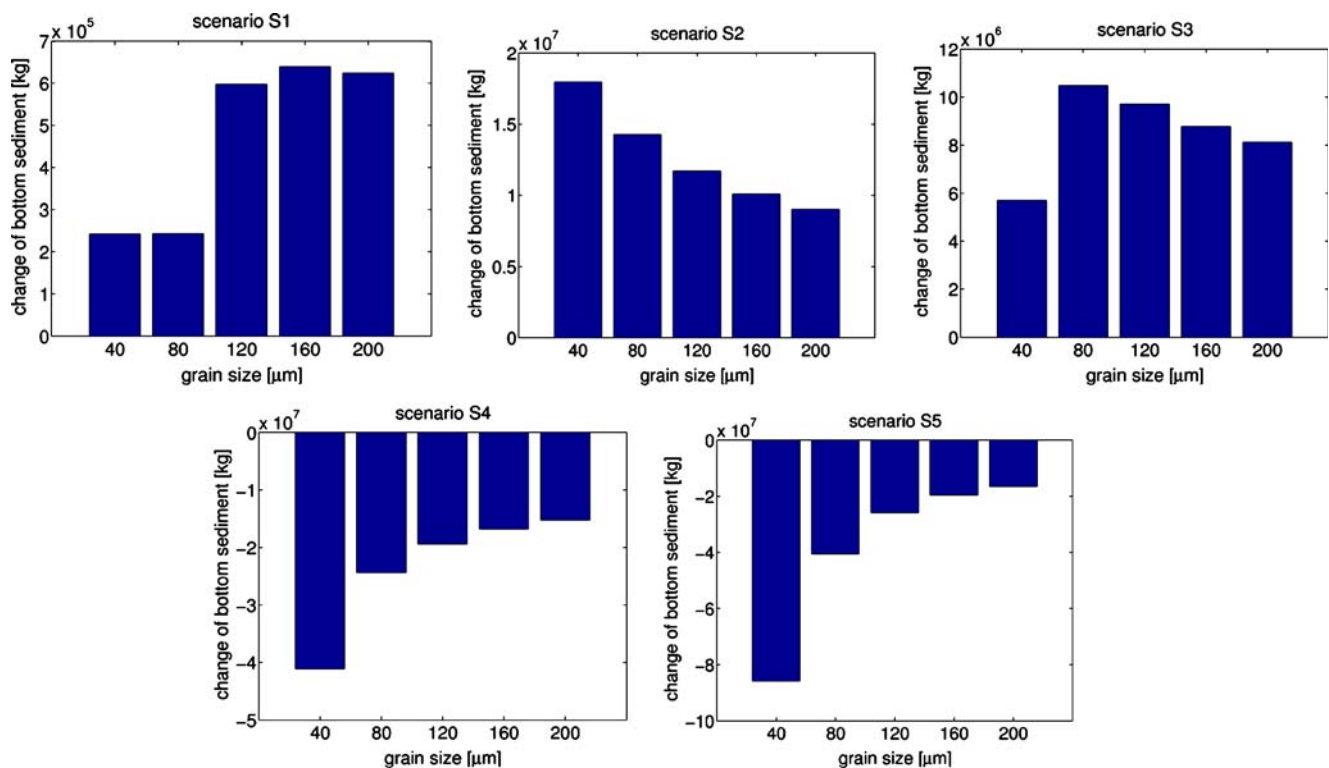


Fig. 12 Change of bottom sediment fractions over three tidal cycles (storm-surge period for scenarios S4 and S5) in the tidal basin area. Positive values denote an accumulation of sediment in the tidal basin area (yellow shading in Fig. 9)

current direction can lead to a relative export of fine sediments from the tidal basin area.

Considering the storm-surge scenarios, especially scenario S5, Figs. 11 and 12 show that there is a net loss of all sediment fractions from the tidal basins, although sediments are imported into the tidal basins via the tidal inlets. This net loss can be explained by an eastward drift of suspended sediment across the eastern boundary (Section 6) due to eastward residual currents that are caused by the strong northwesterly winds. This eastward drift is also visible in scenario S3, where the constant westerly winds also lead to an enhanced sediment export through section 6. Similar to scenario S3, storm surges cause fine sediments to disappear from the tidal basins because, compared to coarser sediments, these are preferentially exported from the tidal basin.

5.3 Change in sediment particle-size distribution

To evaluate the effect of tidal currents and wind-generated waves on the sea bed sediments, the change in sediment grain size for scenarios S1, S2, and S3 is compared in Fig. 13 with measured data in the tidal basin of the island of Spiekeroog. The top left map in that figure depicts the distribution of mean grain size in that basin obtained from Umweltatlas Wattenmeer

(1999). The measured distribution demonstrates two points. The first point is the accumulation of finer sediments close to the mainland coast and the nearly shore-parallel facies belts with increasing grain size from the mainland coast to the barrier island of Spiekeroog. The second point is the accumulation of coarser sediments in the tidal channels between the barrier islands where stronger tidal currents and incoming waves from the open North Sea are present. This is evident in the top left and top right corners of that figure where the mean grain size is larger than $350 \mu\text{m}$.

The other three graphs in Fig. 13 show the change in mean grain size for scenarios S1, S2, and S3. At the beginning of the model integration, the mean grain size was spatially uniform with a mean diameter of $120 \mu\text{m}$ in the whole model area. These figures display the deviation from this initial mean particle size after 9 days of model integration. Obviously, 9 days of model integration is a very short period of time and it cannot be expected that the model results match the observations. On the other hand, an evolutionary trend is evident from these figures. For all three scenarios, an accumulation of coarser sediment can be observed in the main tidal channels close to the openings between the barrier islands. Furthermore, especially in scenario S3, an accumulation of finer sediment begins along the

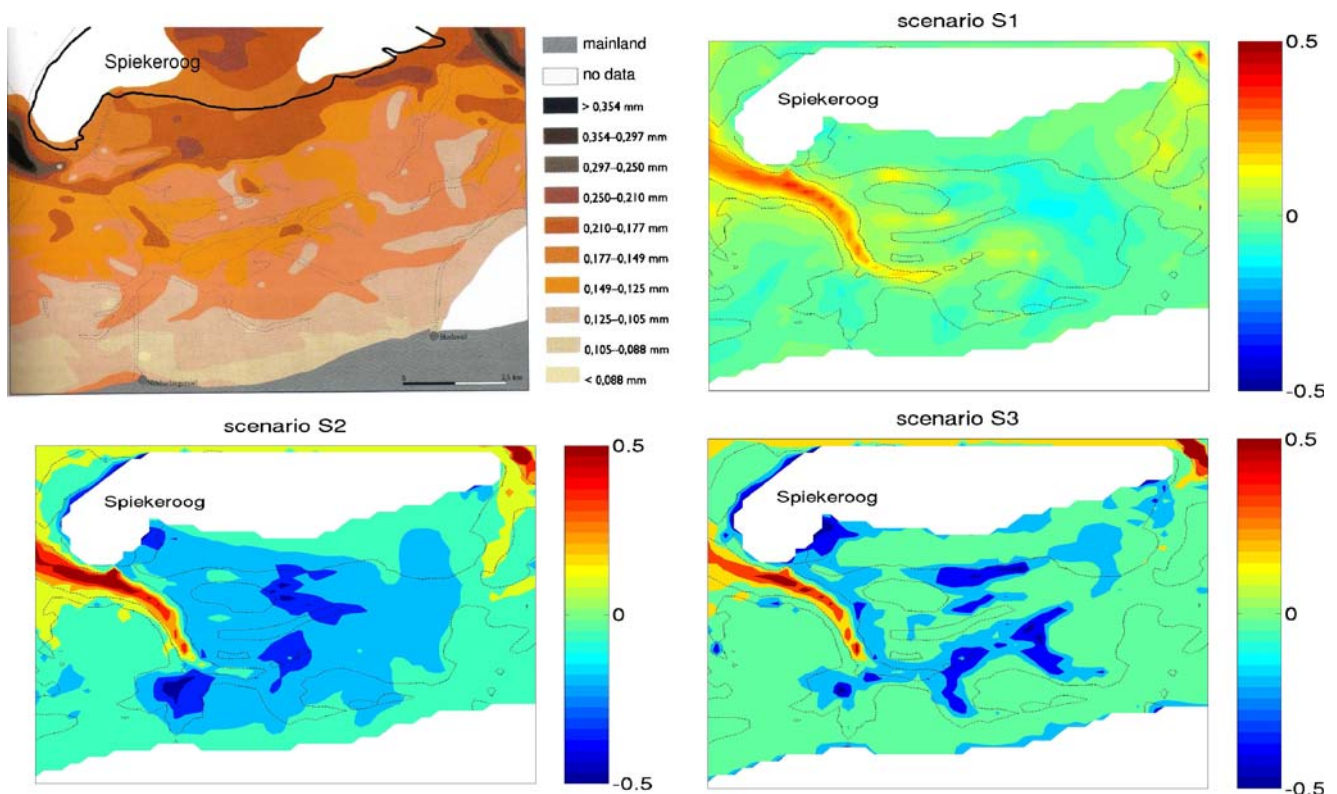


Fig. 13 Spatial distribution of mean grain sizes in the tidal basin of the island of Spiekeroog. The *top left map* depicts measured data displayed in Umweltatlas Wattenmeer (1999). The other three *graphs* show the distribution of the change in mean grain size for scenarios S1, S2, and S3. At the beginning of integration,

the mean grain size was 120 μm in the whole model area. These figures display the deviation from this initial mean particle size after 9 days of model integration. The *thin black lines* denote topographic contours and show the main tidal channels and tidal flats in that region

mainland coast. These trends suggest that the model results capture the right trends. On the other hand, as expected, nine days of model integration is definitely too short to reproduce the measured grain size distributions.

With these sediment size distributions in mind, it is reasonable to add a remark about the calculated budgets of sediment import and export to and from the tidal basins. As stated before, in these modeling studies, there was no lack of any sediment class in the bottom sediment layers during the model integration. This, for example, means that, even in places where fine sediments are rare in nature, e.g., the tidal channels and some regions in front of the barrier islands with high wave activity, they are nevertheless constantly available in the model. Therefore, the import of fine sediments into the tidal basins might be overpredicted in this modeling study, as the model might erode more fine sediments in front of the barrier islands than is actually available there.

On the other hand, the modeling studies show situations where all sediment classes are constantly available

at each location. Given the process study character of the modeling efforts reported here, it is obvious that physical effects such as wave erosion and tidal current energy determine whether sediment is imported into the tidal basins or not. The availability of different sediment classes in the bottom layers is therefore of minor concern in these studies, but it will be considered in the future.

6 Modeling of a strong storm surge

The storm surge on 1 November 2006 caused a sea-level rise that ranges among the three highest sea levels ever recorded along the Lower-Saxonian coastline over the last 100 years (1906, 1962, and 2006). Furthermore, storm Britta caused extremely high waves in the German Bight, as evidenced by structural damage to the FINO1 wind farm research platform (45 km offshore) at heights up to 20 m above the mean sea level (see e.g. Emeis and Türk 2009, and references therein).

The upper two panels in Fig. 14 depict the modeled distribution of significant wave height for the North Sea basin and the East Frisian Wadden Sea for the conditions on 1 November 2006, 01:00 UTC. The lower panels show time series of measured (red) and modeled (blue) significant wave heights at the FINO1 wave buoy in the German Bight (left panel) and at the time-series station in the Wadden Sea (right panel).

As can be seen from these figures, the right order of magnitude and the dynamics of significant wave heights in the Wadden Sea and the German Bight are well captured by the model. However, during storm Britta, the model underestimates the maximum significant wave heights in the German Bight and also overestimates the maximum in the Wadden Sea by approximately 20 cm. This would produce greater sediment erosion in the model on the tidal flats during that storm. The

computation of the significant wave heights could certainly be improved by higher-resolution wind data from the German Weather Service (DWD). The temporal resolution of 6 h of the NCEP/NCAR wind speeds (Kalnay et al. 1996), which were used at the beginning of the numerical experiments, was too coarse to get the right short-term variability in the range of a few hours. Furthermore, the protective influence of the barrier islands with respect to the incoming waves from the North Sea is evident from these graphs.

Measured (top left panel) and modeled (bottom left panel) vertical profiles of current speed at time-series station are presented in Fig. 15 (see Fig. 1 for the position of this station). Compared to the ADCP data, the modeled current speeds show the right magnitude and phase, but there is a notable underestimation of the current speeds during falling water. Especially after the

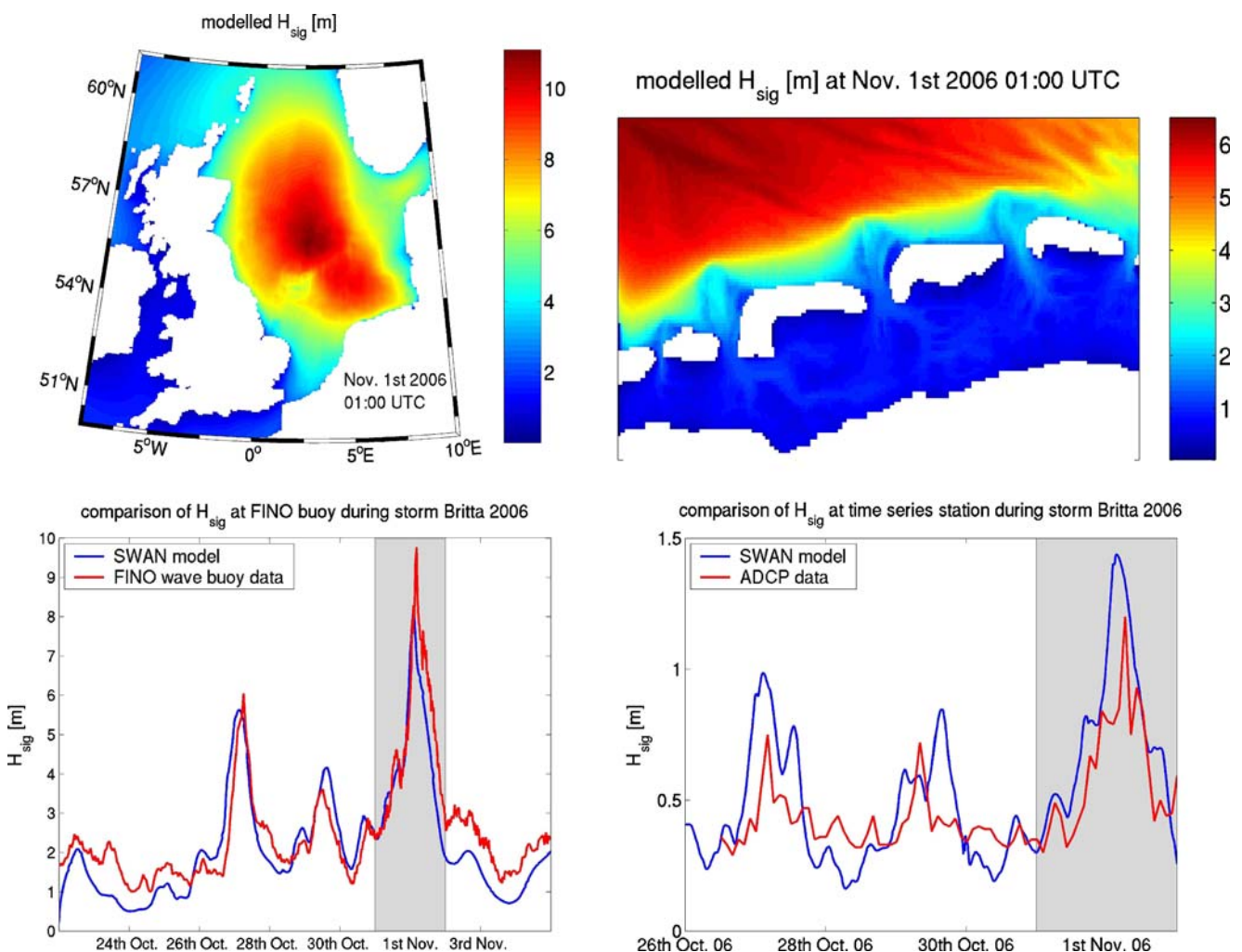


Fig. 14 Comparison of significant wave height (m) during storm Britta in November 2006. The upper graphs present the modeled spatial distribution on 1 November 2006, 01:00 UTC. The lower

graphs show time series of measured and modeled significant wave height at the FINO wave buoy in the German Bight and at the time-series station in the Wadden Sea

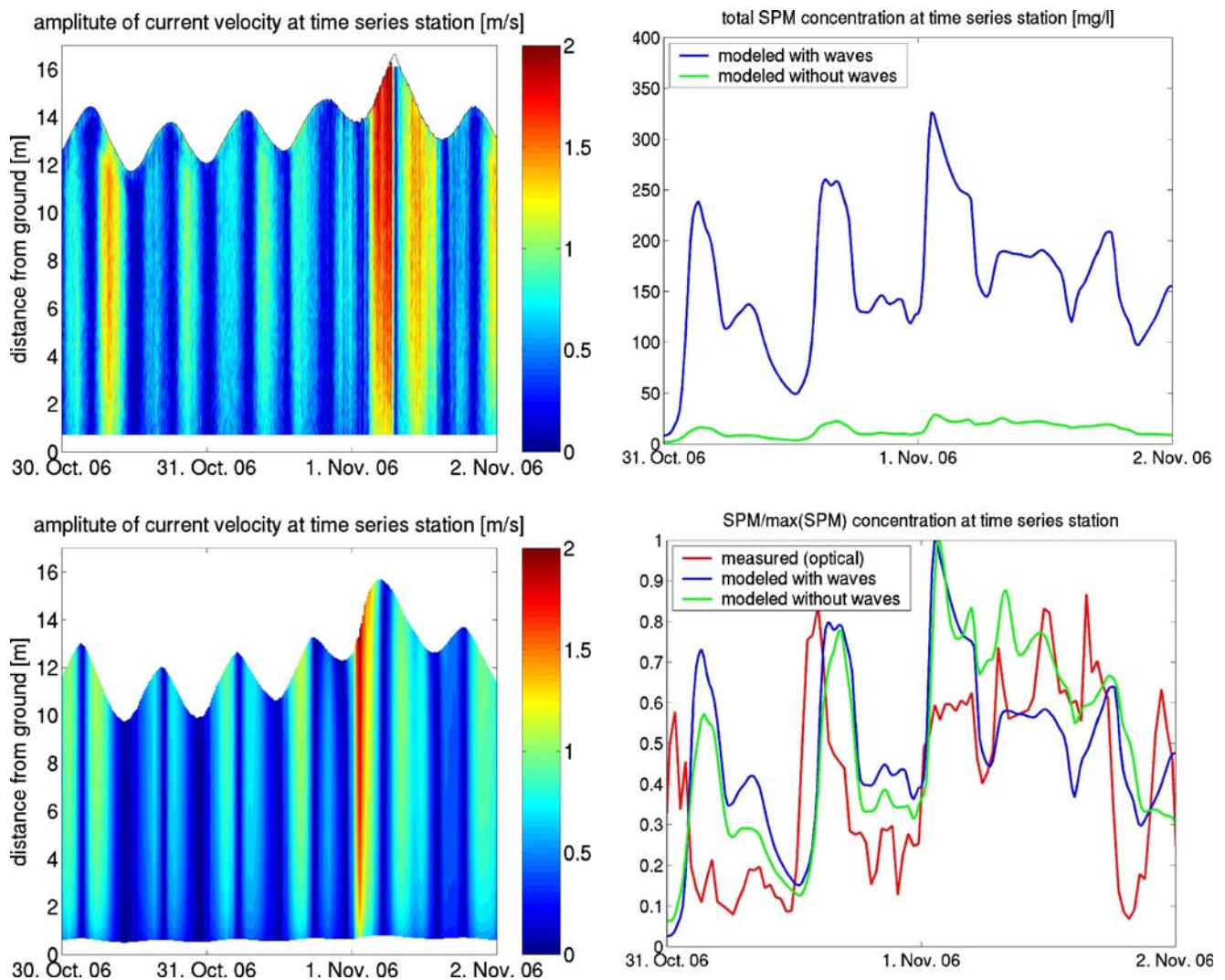


Fig. 15 *Left column:* time-depth plots of current speeds at the time-series station during storm surge Britta in 2006. The *upper graph* shows current speeds from ADCP data, the *lower graph* modeled current speeds. *Right column:* modeled and measured concentrations of suspended matter at the time-series station

during storm Britta in November 2006. In the *lower graph*, the data were normalized to visualize the temporal dynamics. Furthermore, measured data (optical method using a multispectral transmissometer, Badewien et al. 2009) are also depicted

storm surge, when the water is leaving the tidal basins, this discrepancy is unexpectedly large. Obviously, these smaller velocities have an impact on the dynamics of SPM in the model and might lead to an underestimation of the exchange of SPM with the North Sea. Future numerical experiments with improved horizontal resolution and better boundary conditions will help to discriminate between model and observational errors.

Figure 15 also shows suspended sediment concentrations at the time-series station in a fixed water depth during storm Britta. The top graph shows modeled absolute values of SPM concentration with and without the inclusion of wave effects. It is evident from this

graph that wave effects had a tremendous effect on sediment erosion during this storm surge.

In the lower part of this figure, the data were normalized to emphasize the temporal dynamics. In addition, data from a multispectral transmissometer (see Badewien et al. 2009, for more details) are shown, but these optical data still need calibration to be representative for SPM concentration. However, it can be seen that the basic SPM dynamics is captured by the model, although the absolute magnitudes vary substantially. Measurements of suspended sediments in areas that are directly effected by waves, e.g., the shorelines in front of the barrier islands, would be very important

in the future to understand the effect of waves in this region.

6.1 Budgets and transports of SPM through the inlets

In the following, SPM budgets and transports through the inlets and openings of the Wadden Sea region are presented. As mentioned before, the yellow color in Fig. 9 denotes the area for which the change in bottom sediments due to the storm surge was computed. Furthermore, the numbering of the openings to the tidal basins is shown. Sediment transports into the tidal basins are assigned positive values, whereas transports

out of the area are assigned negative values. The time interval associated with the storm surge is from October 31, 12:00 UTC, to November 2, 01:30 UTC. This time interval covers three tidal cycles and is shown as the gray shaded area in the top graphs of Fig. 16.

The top graphs of Fig. 16 show cumulative transports of suspended sediment through the tidal inlet between the islands of Langeoog and Spiekeroog and across section 6 (calculated after Eq. 4). These graphs show that sediments are transported into the tidal basins through the Otzumer Balje (section 4) and sediments leave the area across section 6. This import and export of sediment through the different openings can be seen more clearly in the lower left graph of Fig. 16.

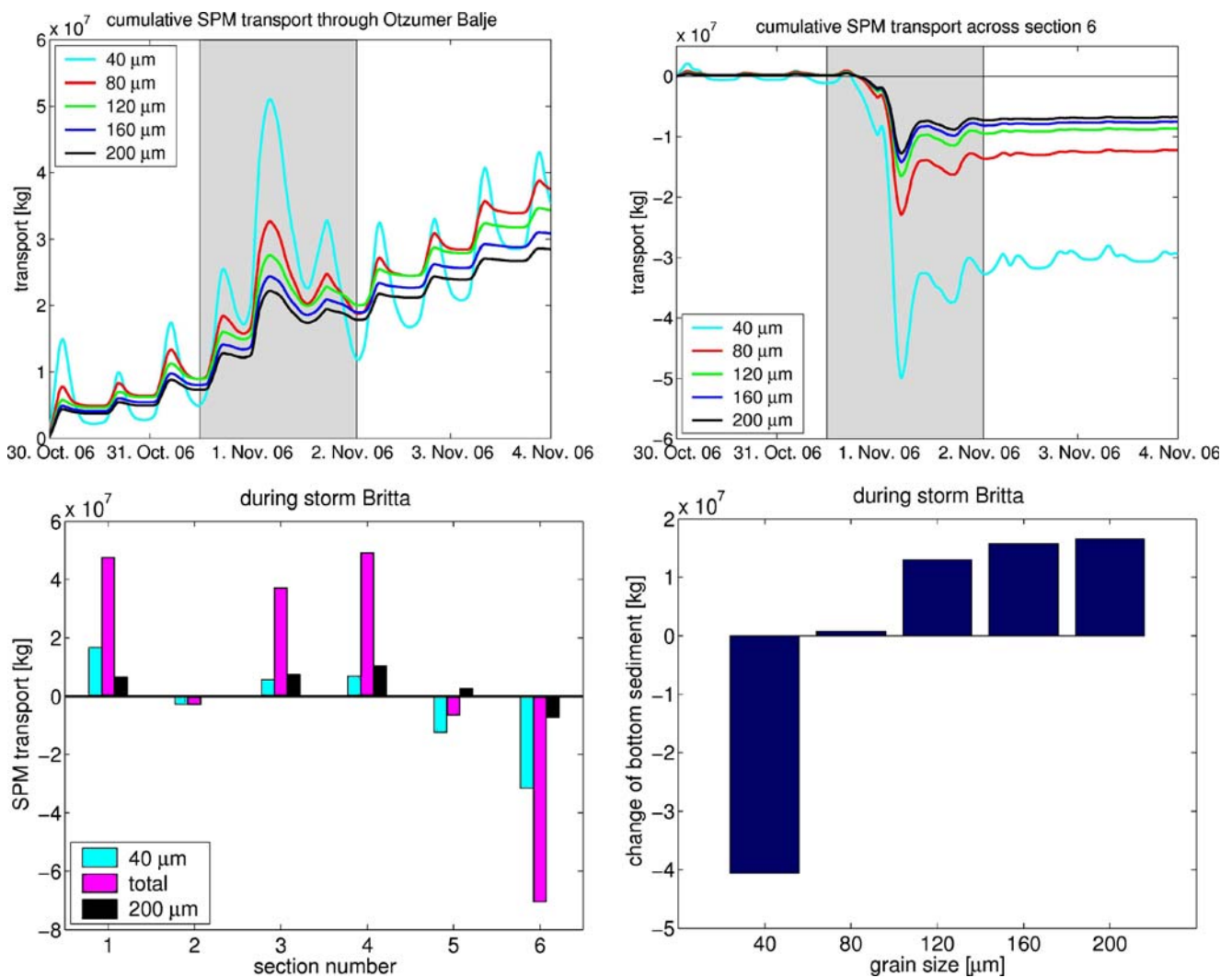


Fig. 16 Upper row: Cumulative transports of suspended sediment fractions through the Otzumer Balje (left) (section 4) and across section 6 (right). Lower row: The left graph shows the time-integrated suspended sediment transports through all open-

ings during the storm surge. The results for the finest sediment fraction, the coarsest sediment fraction, and the total sediment are shown

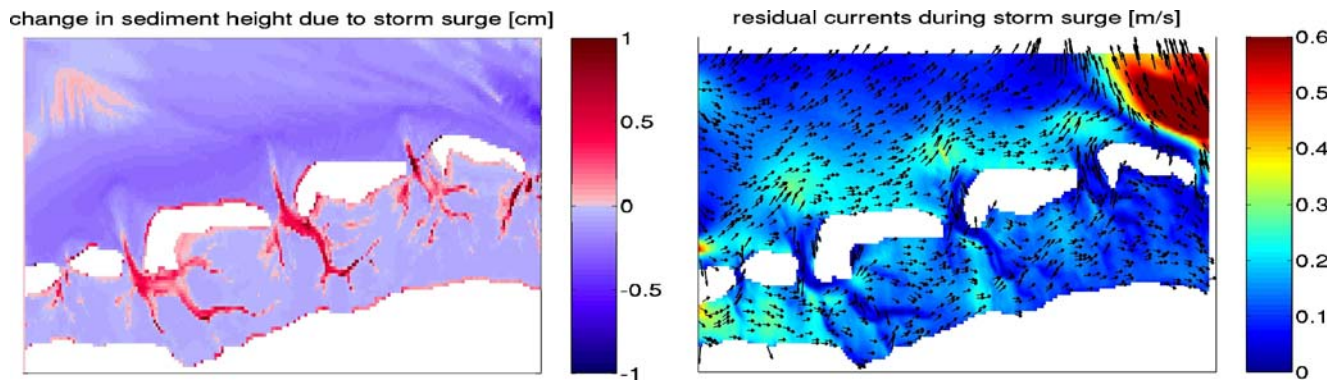


Fig. 17 *Left*: Modeled change of the elevation of bottom sediment layer due to storm Britta in November 2006. A positive change (red color) indicates sediment accumulation. *Right*:

Residual currents during the storm surge. The *arrows* denote the direction of the current and the *color* its magnitude

It illustrates the time-integrated transports across the selected sections during the storm-surge period for the smallest sediment fraction ($40\ \mu\text{m}$), the largest fraction ($200\ \mu\text{m}$), and the total sediment. From this figure, three sections with net import and three sections with net export can be identified. Section 1 is part of the tidal basin area (the East Frisian Wadden Sea extends to beyond this western boundary, see Fig. 1), and therefore, this sediment comes from tidal basins in the west. Through section 6 (close to the eastern boundary), the sediment leaves the Wadden Sea region. The lower right graph of Fig. 16 shows the change of the bottom sediment pools during the storm surge in the tidal basin area (yellow area in Fig. 9). It is obvious that the coarser sediments accumulate in the tidal basin region, whereas the smallest sediment fraction is flushed out of the tidal basins. Interestingly, the coarser sediments are brought into the basins through openings 1–5 and deposit in the tidal basin area. Only a small part leaves the tidal basin across section 6. One reason for the eastward drift of SPM is the northwesterly winds during the storm surge, which result in a mainly eastward-directed residual current field (see right graph of Fig. 17)

The loss of the fine bottom sediment fraction is of the order of $4 \cdot 10^7\ \text{kg}$ in the tidal basin area, whereas the accumulation of coarser sediments is $3.5 \cdot 10^7\ \text{kg}$. This results in a net loss of $0.5 \cdot 10^7\ \text{kg}$ of total sediment mass from the considered area during the time period of storm Britta.

6.2 Storm-surge induced change in bottom morphology

In Fig. 17, the change in the bottom sediment layer thickness due to the storm surge is calculated (assuming

a sediment porosity of 0.4).¹ Sediment erosion takes place on the tidal flats and in front of the barrier islands where the waves are very strong. A net accumulation in the tidal channels and close to the shorelines can be observed. At first sight, this net accumulation of sediments in the tidal channels might be unrealistic if one considers the high erosion potential of tidal currents depicted in Fig. 8. On the other hand, it was also demonstrated that due to the storm surge, and especially due to the high wave action in front of the barrier islands and over the tidal flats, that there is a huge amount of suspended sediment in the water column. These sediments are transported to the tidal channels during falling water and can deposit in these channels once the storm moderates. Therefore, the model results suggest that storm surges tend to smoothen the topography of tidal basins by reworking and redistribution of sediments.

The modeled change in thickness of the bottom layer is of the order of a few centimeters, which seems to be very low. However, this change in elevation must be viewed in the light of the relatively coarse horizontal model resolution of 200 m used in these numerical experiments.

7 Summary and conclusions

A numerical modeling system based on the hydrodynamical model GETM of Burchard and Bolding (2002) and the third-generation wave model SWAN of Booij

¹To transform the mass change of bottom sediment into a change in the thickness of the bottom sediment layer, the porosity of the sediment must be considered. With the mass change ΔM measured in kilograms per square meter, the sediment density ρ_S , and sediment porosity ϕ , the elevation change Δz is calculated by $\Delta z = \Delta M / ((1 - \phi) \rho_S)$.

et al. (1999) was used to investigate the effects of wind-generated surface gravity waves, tidal currents, and storm surges on SPM dynamics in the East Frisian Wadden Sea, southern North Sea.

Model results were compared with observations of significant wave height, current speeds, and suspended sediment concentration obtained during two ship cruises, from a time-series station located in the study area, and from wave buoys located in the German Bight close to the study area. Artificial and idealized forcing functions of wind speed, sea surface elevation, and significant wave height were used to discriminate the different effects of tidal currents, wind-generated surface waves, and storm surges. Finally, the effect of a real storm surge caused by storm Britta in November 2006 on the sedimentary system of the Wadden Sea was hindcasted.

The artificial scenarios demonstrated that, under normal and moderate weather conditions (scenarios S1–S3), tidal currents are most effective in eroding sediments in this region. The main locations of erosion in these cases are the tidal inlets between the barrier islands and the tidal channels. The influence of waves is very important in front of the barrier islands and (during high-wind scenarios) on the tidal flats.

For windy weather conditions, the artificial scenarios S1 to S3 support the theory proposed by Santamarina Cuneo and Flemming (2000) that erosion due to waves in front of the barrier islands should lead to an enhanced import of suspended sediment into the tidal basins. Besides other mechanisms, e.g., the settling/scour lag effect, which are usually proposed as a cause for sediment accumulation in tidal basins, it is demonstrated that this mechanism proposed by Santamarina Cuneo and Flemming (2000) also contributes to an accumulation of sediments in the considered tidal basins.

During storm-surge conditions, waves have the most dominant effect on SPM dynamics. In front of the barrier islands, sediments are eroded by wave action and are transported into the tidal basins by the currents. Furthermore, sediment erosion due to waves is significantly enhanced on the tidal flats. The eroded sediments are transported out of the tidal basin area, especially for the fine sediment fractions due to their lower settling speeds. Therefore, during storm surges, the Wadden Sea especially loses the smaller-sized fractions, which supports the hypothesis of Santamarina Cuneo and Flemming (2000).

The results of the numerical experiments with forcing data for the situation during storm Britta are quite similar to scenario S5. In this case, a net loss of sediment from the tidal basins can be seen in the model results,

mainly due to enhanced sediment erosion by waves and eastward residual currents transporting the sediments through the eastern section. This net loss is highest for the finest sediment fraction, whereas the coarser sediment fractions show slight accumulations within the tidal basins. During this storm, the coarser sediment is imported into the tidal basins through the northern tidal inlets, where they accumulate due to their higher settling velocities.

The results of this study demonstrate that the modeling system used in this study is capable of modeling the dynamics of wave parameters, current speeds, and sediment concentrations in the East Frisian Wadden Sea. Future studies will have to include effects of cohesion in the sediment module and wave–current interaction in the coupled hydrodynamic-wave module.

Acknowledgements This model study was highly dependent on external data sources. Therefore, we are grateful to Ralf Berger from the Federal Maritime and Hydrographic Agency (BSH, *Bundesamt für Seeschifffahrt und Hydrographie*) for providing the wave data from the wave buoys in the German Bight; Heike Gentz and Michael Hesse from BSH and Ralf Kaiser from NLWKN (Niedersächsischer Landesbetrieb für Wasserwirtschaft, Küsten- und Naturschutz) for bathymetric data; and, finally, Adam Kubicki (Forschungsinstitut Senckenberg, Department of Marine Science) for providing us with wave data from the time-series station. Furthermore, we want to mention the helpful discussions with Alexander Bartholomä, Burghard Flemming, Jöran März, Ulf Gräwe, Joanna Staneva, and Emil Stanev. Last but not least, we thank two anonymous reviewers, whose thoughtful comments helped to improve the quality of the manuscript. This study was embedded within the research group 'Biogeochemistry of tidal flats', which was funded by the *Deutsche Forschungsgemeinschaft* (DFG).

Appendix

SPM transport module

The SPM transport module used in this study is described here in more detail. For each sediment fraction c^i , the usual diffusion–advection equation can be written as

$$\begin{aligned} \partial_t c^i + \partial_x(uc^i) + \partial_x(v c^i) + \partial_z((w - w_s^i)c^i) = \\ \partial_x(A_h \partial_x c^i) + \partial_y(A_h \partial_y c^i) + \partial_z(A_v \partial_z c^i) \end{aligned} \quad (5)$$

Here, u , v , and w denote current speeds in the three cartesian directions; w_s^i denotes the settling velocity of the i^{th} particle fraction; and A_v and A_h denote the vertical and horizontal eddy diffusivity.

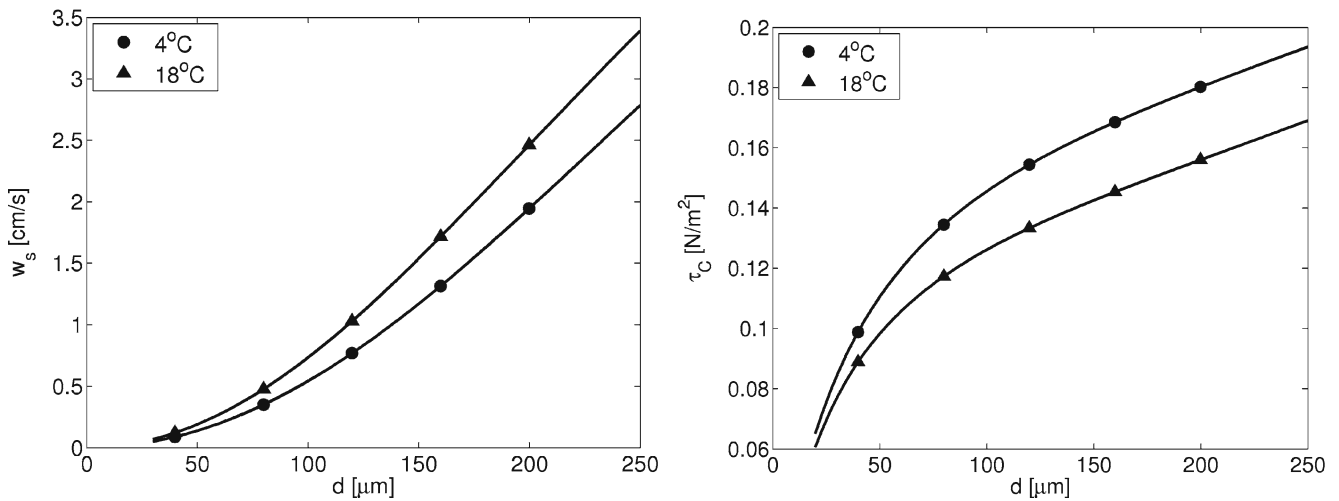


Fig. 18 *Left*: settling velocity of sand grains as a function of grain diameter after Soulsby (1997) (see Eq. 9). *Right*: critical shear stress as a function of grain diameter after Soulsby and Whitehouse (1997) (see Eq. 13)

While the horizontal diffusivity A_h was set constant, the vertical diffusivity A_v was a combination of three components:

$$A_v(z) = A_v^t(z) + A_v^W(z) + A_v^b \tag{6}$$

$A_v^t(z)$ accounted for the vertical turbulent diffusion induced by the current field and was calculated by the General Ocean Turbulence Model (GOTM, Burchard et al. 1999), which is part of the GETM model. A_v^b denotes the constant background diffusivity, which, in contrast to the turbulent diffusivity $A_v^t(z)$, was also present when there was no motion of the water column. In this model study, a value of $A_v^b = 1.0 \cdot 10^{-6} \text{ m}^2/\text{s}$ was used.

To include the effect of surface gravity waves on the vertical diffusion of SPM, a parameterization proposed by Pleskachevsky et al. (2005) was implemented, which is based on the wave induced-orbital velocity field:

$$A_v^W(z) = (k \cdot H_{\text{sig}})^2 \cdot U_w(z)^2 \cdot T_{\text{peak}} \tag{7}$$

Here, H_{sig} denotes the significant wave height, T_{peak} the peak period of the underlying wave spectrum, k the corresponding wave number according to the dispersion relation of surface gravity waves (a formula to calculate the wave number is given below in Eq. 18), and $U_w(z)$ the amplitude of the wave-induced orbital velocity, which is given by:

$$U_w(z) = \frac{\pi H_{\text{sig}} \cosh(k(h+z))}{T_{\text{peak}} \sinh(kh)}, \tag{8}$$

where h denotes the water depth measured downward from the surface (the bottom level is $z = -h$).

The settling velocity of the i^{th} particle fraction was calculated after a formula from Soulsby (1997), which is valid for noncohesive irregular sand grains (Table 3):

$$w_s^i = \frac{\nu}{d} \left\{ \sqrt{10.36^2 + 1.049 D_s^3} - 10.36 \right\} \tag{9}$$

$$D_s = \left[\frac{g}{\nu^2} \left(\frac{\rho_s}{\rho_w} - 1 \right) \right]^{1/3} d$$

Here, g denotes the acceleration due to gravity, ρ_s and ρ_w the sediment and water density in kilograms per cubic meter, ν the kinematic viscosity in square meters per second, and d the sediment diameter in meters (see left graph in Fig. 18).

The temperature dependency of the kinematic viscosity ν was calculated by:

$$\nu = \frac{1}{\rho_w} \eta \exp\left(\frac{b}{T + 273.0}\right), \tag{10}$$

with temperature T in $^{\circ}\text{C}$, $\eta = 1.9909 \cdot 10^{-6} \text{ kg}/(\text{ms})$, and $b = 1.8284 \cdot 10^3 \text{ K}$.

In the vertical direction, sediment only entered and left the water column through the bottom boundary

Table 3 Settling velocities at 4°C and critical shear stress for the different sediment fractions after Eqs. 9 and 13

$d [\mu\text{m}]$	$w_s [\text{cm}/\text{s}]$	$\tau_c [\text{N}/\text{m}^2]$
40	0.09	0.10
80	0.35	0.13
120	0.77	0.15
160	1.32	0.17
200	1.95	0.18

layer, for which the following sediment flux condition was used:

$$(A_b \partial_z c^i + w_s^i c^i)_{z=-h} = F_{\text{ero}}^i - F_{\text{dep}}^i \tag{11}$$

Here, F_{ero} and F_{dep} denote the sediment fluxes at the bottom due to erosion and deposition.

According to Einstein and Krone (1962), the deposition flux was calculated with:

$$F_{\text{dep}}^i = \begin{cases} w_s^i \cdot c^i_{z=-h} \left(\frac{\tau_B}{\tau_c^i} - 1 \right) & \tau_B < \tau_c^i \\ 0 & \tau_B > \tau_c^i \end{cases} \tag{12}$$

Here, τ_B denotes the bottom shear stress and τ_c^i a critical shear stress, which had to be reached by the fluid in order to erode sediment from the bottom into the water column. If the bottom shear stress was below that value, suspended sediment settled to the bottom. Soulsby and Whitehouse (1997) provided an empirical formula for that critical shear stress, which is given by (Table 3):

$$\tau_c = g d (\rho_s - \rho_w) \theta_c \tag{13}$$

$$\theta_c := \frac{0.3}{1 + 1.2 D_s} + 0.055 (1 - \exp(-0.02 D_s))$$

In Fig. 18, the critical shear stress is depicted for two different water temperatures. It is evident from this figure that the critical shear stresses used in this study are of the same order as those reported by Austen and Witte (2000) for sandy sediments in the Wadden Sea region. However, these values do not account for muddy and cohesive sediments, which have higher critical shear stresses of about 0.5–1.0 N/m². This effect will be implemented in a future study.

Furthermore, to determine the critical shear stress for a particular sediment fraction, the bottom sediments were modeled as separate pools that did not interact with each other. Therefore, the different sediment fractions were eroded and deposited separately from each other without accounting for mean grain size and mean critical shear stress at a specific location.

The erosion flux was calculated according to the formula of Partheniades (1965):

$$F_{\text{ero}}^i = \begin{cases} M_e \left(\frac{\tau_B}{\tau_c^i} - 1 \right) & \tau_B > \tau_c^i \\ 0 & \tau_B < \tau_c^i \end{cases} \tag{14}$$

M_e is a free parameter that can be adapted to measurements of sediment concentration. For their studies in the East Frisian Wadden Sea, Stanev et al. (2006) used a value of $M_e = 3.7 \cdot 10^{-6}$ kg/(m²s).

Total bottom shear stress responsible for sediment erosion and deposition was modeled as a nonlinear

combination of a current-induced component τ_{current} and a wave-induced component τ_{wave} (Soulsby 1997). This approach was also used by Pleskachevsky et al. (2005) and Gayer et al. (2006):

$$\tau_B = [(\tau_m + \tau_{\text{wave}} \cos(\phi))^2 + (\tau_{\text{wave}} \sin(\phi))^2]^{1/2} \tag{15}$$

$$\tau_m := \tau_{\text{current}} \left[1 + 1.2 \left(\frac{\tau_{\text{wave}}}{\tau_{\text{wave}} + \tau_{\text{current}}} \right)^{3.2} \right]$$

Here, ϕ denotes the angle between the direction of wave propagation and current flow.

The current-induced bottom shear stress was calculated in GETM via an iterative procedure with a prescribed constant bottom roughness length z_0 (see more details in Burchard and Bolding (2002)).

The wave-induced component was calculated after an approach proposed by Soulsby (1997). This approach begins with a general relation for bottom shear stress due to surface gravity waves:

$$\tau_{\text{wave}} = \frac{1}{2} \rho_w f_w U_w^2 \tag{16}$$

Here, f_w denotes the wave friction factor, ρ_w the water density, and U_w the horizontal wave orbital velocity near the bottom just above the wave boundary layer. The bottom velocity was approximated by:

$$U_w = \frac{\pi H_{\text{sig}}}{T_{\text{peak}} \sinh(kh)}, \tag{17}$$

which is the bottom velocity expression of Airy-waves. Here, h denotes the water depth, H_{sig} the wave height, T_{peak} the wave period, and k the corresponding wave number.

In general, the wave number is related to the peak period by the dispersion relation of surface gravity waves:

$$\frac{2\pi}{T_{\text{peak}}} = g k \tanh(kh)$$

However, as it is not straightforward to obtain the wave number k from this dispersion relation if only T_{peak} is known, a simple estimation provided by Soulsby (1997) was used in this study:

$$k = \begin{cases} \frac{1}{h} \left(\frac{4\pi^2 h}{T_{\text{peak}}^2 g} \right)^{1/2} \left(1 + 0.2 \cdot \frac{4\pi^2 h}{T_{\text{peak}}^2 g} \right) & , \text{ for } \frac{4\pi^2 h}{T_{\text{peak}}^2 g} \leq 1 \\ \frac{1}{h} \frac{4\pi^2 h}{T_{\text{peak}}^2 g} \left[1 + 0.2 \cdot \exp \left(2 - 2 \cdot \frac{4\pi^2 h}{T_{\text{peak}}^2 g} \right) \right] & , \text{ for } \frac{4\pi^2 h}{T_{\text{peak}}^2 g} > 1 \end{cases} \tag{18}$$

The wave friction factor f_w was calculated for f_{ws} in the case of smooth beds or f_{wr} in the case of rough beds by:

$$f_{wr} = 1.39 \left(\frac{A}{z_0} \right)^{-0.52}, \quad f_{ws} = B R_w^{-N} \quad (19)$$

The bottom roughness was calculated by $z_0 = d_{50}/12$ and the semiorbital excursion A was given by $A = U_w T_{\text{peak}} / (2\pi)$. The parameters of the smooth bed friction factor f_{ws} were dependent on the turbulence of the motion, which could be determined from the wave Reynolds number $R_w = U_w A / \nu$. According to this number, the parameters N and B were calculated by:

$$B = 2; N = 0.5 \quad \text{if } R_w \leq 5 \cdot 10^5 \text{ (laminar)} \quad (20)$$

$$B = 0.0521; N = 0.187 \text{ if } R_w > 5 \cdot 10^5 \text{ (smooth turbulent)} \quad (21)$$

Finally, if sediments were deposited at or eroded from the bottom, the mass of the available sediment pools changed. Each bottom pool P_B^i was changed according to the following equation:

$$\partial_t P_B^i = F_{\text{dep}}^i - F_{\text{ero}}^i \quad (22)$$

References

- Austen I, Witte G (2000) Comparison of the erosion shear stress of oxic and anoxic sediments in the East Frisian Wadden sea. In: Flemming BW et al (ed) (2000) Muddy coast dynamics and resource management. Proceedings in Marine Science, vol 2. Elsevier, Amsterdam, pp 75–84
- Badewien TH, Zimmer E, Bartholomä A, Reuter R (2009) Time series measurements of suspended particulate matter (SPM) in turbid coastal waters. *Ocean Dyn*. doi:10.1007/s10236-009-0183-8
- Bartholdy J, Anthony D (1998) Tidal dynamics and seasonal dependent import and export of fine-grained sediment through a backbarrier tidal channel of the Danish Wadden Sea. In: Tidalities: processes and products, SEPM, special publication, vol 61. SEPM, Tulsa, pp 43–52
- Bassoullet P, Le Hir P, Gouleaub D, Robert S (2000) Sediment transport over an intertidal mudflat: field investigations and estimation of fluxes within the 'Baie de Marenngres-Oleron' (France). *Cont Shelf Res* 20:1635–1653
- Blaas M, Changming D, Marchesiello P, McWilliams JC, Stolzenbach K (2007) Sediment-transport modeling on southern californian shelves: a ROMS case study. *Cont Shelf Res* 27:832–853
- Booij N, Ris RC, Holthuijsen LH (1999) A third-generation wave model for coastal regions 1. model description and validation. *J Geophys Res* 104:7649–7666
- Burchard H, Bolding K (2002) GETM—a general estuarine transport model. Sci Doc EUR 20253 EN, Inst for Environ and Sustainability, Ispra, Italy
- Burchard H, Bolding K, Villarreal MR (1999) GOTM—a general ocean turbulence model. theory, applications and test cases. Tech Rep EUR 18745 EN, European Commission
- Burchard H, Bolding K, Villereal M (2004) Three-dimensional modelling of estuarine turbidity maxima in a tidal estuary. *Ocean Dyn* 54:250–265
- Burchard H, Bolding K, Umlauf L (2007) GETM—General Estuarine Transport Model, source code and test case documentation. <http://www.getm.eu>
- Burchard H, Flüser G, Staneva J, Badewien TH, Riethmüller R (2008) Impact of density gradients on net sediment transport into the wadden sea. *J Phys Oceanogr* 38:566–587
- Cavaleri L, Malanotte-Rizzoli P (1981) Wind wave prediction in shallow water: theory and application. *J Geophys Res* 86:10961–10973
- Chang TS, Joerdel O, Flemming BW, Bartholomä A (2006) The role of particle aggregation/disaggregation in muddy sediment dynamics and seasonal sediment turnover in a backbarrier tidal basin, East Frisian Wadden Sea, southern North Sea. *Mar Geol* 235:49–61
- Condie SA, Sherwood CR (2006) Sediment distribution and transport across the continental shelf and slope under idealized wind forcing. *Prog Oceanogr* 70:255–270
- Einstein HA, Krone RB (1962) Experiments to determine modes of cohesive sediment transport in salt water. *J Geophys Res* 67:1451–1461
- Emeis S, Türk M (2009) Wind-driven wave heights in the German Bight. *Ocean Dyn*. doi:10.1007/s10236-008-0178-x
- ETOPO2 (2006) 2-minute Gridded Global Relief Data (ETOPO2v2). US Department of Commerce, National Oceanic and Atmospheric Administration, National Geophysical Data Center
- Flemming BW, Nyandwi N (1994) Land reclamation as a cause of fine-grained sediment depletion in backbarrier tidal flats (southern North Sea). *Neth J Aquat Ecol* 28:299–307
- Flemming BW, Ziegler K (1995) High-resolution grain size distribution patterns and textural trends in the backbarrier environment of Spiekeroog Island (southern North Sea). *Senckenb Marit* 26:1–24
- Gayer G, Dick S, Pleskachevsky A, Rosenthal W (2006) Numerical modeling of suspended matter transport in the north sea. *Ocean Dyn* 56:62–77
- Holthuijsen LH (2007) Waves in Oceanic and Coastal Waters. Cambridge University Press, Cambridge
- Kalnay et al (1996) The NCEP/NCAR 40-year reanalysis project. *Bull Am Meteorol Soc* 77:437–470
- Komen G, Hasselmann K, Hasselmann K (1984) On the existence of a fully developed wind-sea spectrum. *J Phys Oceanogr* 14:1271–1285
- Krögel F, Flemming BW (1998) Evidence for temperature-adjusted sediment distributions in the back-barrier tidal flats of the East Frisian Wadden Sea (southern North Sea). In: Alexander CR, Davis RA, Henry VJ (eds) In: Tidalities: processes and products, SEPM, special publication, vol 61. SEPM, Tulsa, pp 31–41
- Liang BC, Li HJ, Lee DY (2007) Numerical study of three-dimensional suspended sediment transport in waves and currents. *Ocean Eng* 34:1569–1583
- Loewe P, Klein H, Becker G, Nies H, Brockmann U, Schmolke S, Dick S, Schrader D, Frohse A, Schulz A, Herrmann J, Theobald N, Klein B, Weigelt S (2006) Nordseezustand 2004. Berichte des Bundesamtes für Seeschifffahrt und Hydrographie (BSH) 40
- Partheniades E (1965) Erosion and deposition of cohesive soils. *Proc ASCE J Hydraul Div* 91:105–139

- Pleskachevsky A, Gayer G, Horstmann J, Rosenthal W (2005) Synergy of satellite remote sensing and numerical modeling for monitoring of suspended particulate matter. *Ocean Dyn* 55:2–9
- Roberts W, Le Hir P, Whitehouse RJS (2000) Investigation using simple mathematical models of the effect of tidal currents and waves on the profile shape of intertidal mudflats. *Cont Shelf Res* 20:1079–1097
- Santamarina Cuneo P, Flemming BW (2000) Quantifying concentration and flux of suspended particulate matter through a tidal inlet of the East Frisian Wadden Sea by acoustic doppler current profiling. In: Flemming, BW et al (eds) (2000) *Muddy coast dynamics and resource management*. Proceedings in Marine Science vol 2. Elsevier, Amsterdam, pp 39–52
- Soulsby R (1997) *Dynamics of marine sands. a manual for practical applications*. Thomas Telford, London
- Soulsby R, Whitehouse R (1997) Threshold of sediment motion in coastal environments. Proc Pacific Coasts and Ports '97 Conf, Christchurch, 1, University of Canterbury, New Zealand pp 149–154
- Stanev EV, Wolff J-O, Burchard H, Bolding K, Flöser G (2003) On the circulation in the East Frisian Wadden Sea: numerical modeling and data analysis. *Ocean Dyn* 53: 27–51
- Stanev EV, Flöser G, Wolff J-O (2003b) First- and higher-order dynamical controls on the water exchanges between tidal basins and the open ocean. a case study for the East Frisian Wadden Sea. *Ocean Dyn* 53:146–165
- Stanev EV, Wolff J-O, Brink-Spalink G (2006) On the sensitivity of the sedimentary system in the East Frisian Wadden Sea to sea-level rise and wave-induced bed shear stress. *Ocean Dyn* 56:266–283
- Stanev EV, Brink-Spalink G, Wolff J-O (2007) Sediment dynamics in tidally dominated environments controlled by transport and turbulence: a case study for the East Frisian Wadden Sea. *J Geophys Res* 112
- Staneva J, Stanev EV, Wolff J-O, Badewien TH, Reuter R, Flemming B, Bartholomä, Bolding K (2008) Hydrodynamics and sediment dynamics in the German Bight. A focus on observations and numerical modelling in the East Frisian Wadden Sea. *Cont Shelf Res* 29(1):302–319
- Umweltatlas Wattenmeer (1999) Band 2, Wattenmeer zwischen Elb- und Emsmündung. Ulmer Verlag Stuttgart, Germany
- van Straaten LMJU, Kuenen PH (1957) Accumulation of fine grained sediments in the Dutch Wadden Sea. *Geol Mijnb* 19:329–354
- Warner JC, Butman B, Soupy Dalyander P (2008) Storm-driven sediment transport in Massachusetts bay. *Cont Shelf Res* 28:257–282